NASA
Technical
Paper
3010

November 1990

Free Vibrations of Thin-Walled Semicircular Graphite-Epoxy Composite Frames

Ahmed K. Noor, Huey D. Carden,
and Jeanne M. Peters

NASA

NASA Technical Paper 3010

1990

Free Vibrations of Thin-Walled Semicircular Graphite-Epoxy Composite Frames

Ahmed K. Noor
The George Washington University
Joint Institute for Advancement of Flight Sciences
Langley Research Center
Hampton, Virginia

Huey D. Carden
Langley Research Center
Hampton, Virginia

Jeanne M. Peters
The George Washington University
Joint Institute for Advancement of Flight Sciences
Langley Research Center
Hampton, Virginia

NASA
National Aeronautics and Space Administration
Office of Management
Scientific and Technical Information Division

The use of trademarks or names of manufacturers in this report is for accurate reporting and does not constitute an official endorsement, either expressed or implied, of such products or manufacturers by the National Aeronautics and Space Administration.

Contents

Abstract

A detailed study is made of the effects of variations in lamination and material parameters of thin-walled composite frames on their vibrational characteristics. The structures considered are semicircular thin-walled frames with I and J sections. The flanges and webs of the frames are modeled by using two-dimensional shell and plate finite elements. A mixed formulation is used with the fundamental unknowns consisting of both the generalized displacements and stress resultants in the frame. The frequencies and modes predicted by the two-dimensional finite-element model are compared with those obtained from experiments, as well as with the predictions of a one-dimensional, thin-walled-beam, finite-element model. A detailed study is made of the sensitivity of the vibrational response to variations in the fiber orientation, material properties of the individual layers, and boundary conditions.

Introduction

The physical understanding and the numerical simulation of the dynamic response of laminated anisotropic structures have recently become the focus of intense efforts because of the expanded use of fibrous composites in the aerospace, automotive, shipbuilding, and other industries, and because of the need to establish the practical limits of the dynamic load-carrying capability of structures made from these materials. Experimental studies have been conducted on the free vibration and impact response of thin-walled composite frames and stiffeners (e.g., see Boitnott et al. 1987; Boitnott and Fasanella 1989; Collins and Johnson 1989; and Chandra, Ngo, and Chopra 1988). One-dimensional theories have been developed for the static, vibration, and buckling analyses of thin-walled-frame structures (e.g., Vlasov 1961; Gjelsvik 1981; Nowinski 1966; and Panovko and Beilin 1969). However, no systematic assessment has been made of the range of validity of the basic assumptions of these theories. Approximate analytical and numerical techniques have been applied to the study of the vibrational response of isotropic and composite stiffeners (e.g., see Hasan and Barr 1974; Vermisyan and Galin 1972; Rao 1975; Vasilenko and Trivailo 1980; Narayanan, Verma, and Mallik 1981; Ali 1984; Gupta, Venkatesh, and Rao 1985; Potiron et al. 1985; Rückschloss 1985; Wekezer 1987; Rehfield, Atilgan, and Hodges 1990; Stemple and Lee 1988; and Bishop, Cannon, and Miao 1989). Few publications exist in which the effects of variations in lamination and geometric parameters of composite panels on their vibrational characteristics are studied (see Teh and Huang 1980 and Bank and Kao 1989). However, none of these publications consider thin-walled composite frames.

The present study is an attempt to fill this void. Specifically, the objective of this paper is to summarize the results of a recent study on the effects of variations in the lamination and of geometric parameters of thin-walled composite frames on their vibrational characteristics (frequencies, and energy components associated with different modes). The frames considered are semicircular, are made of thin-walled graphite-epoxy material with I and J sections, and have a 36-in. radius (see fig. 1).

Symbols

A	cross-sectional area of one-dimensional-beam model
A_y, A_z	effective shear areas for one-dimensional-beam model in y- and z-directions, respectively
A_{11}	extensional stiffness of laminate (flanges or web) in x_1-direction
A_{33}	in-plane shear stiffness of laminate
B_ω	bimoment in one-dimensional-beam model
b, b_1, b_2, b_3, b_4	flange (or skin) dimensions (see tables 2 and 3)
c_i	multipliers (see eqs. (5) and (7))
d, d_1, d_2	web dimensions (see tables 2 and 3)
E, G	effective Young's and shear moduli of equivalent isotropic material
E_L, E_T	elastic moduli of individual layers of laminate (flanges or web) in direction of fibers and normal to it, respectively
$[F]$	matrix of linear flexibility coefficients for an individual element
G_{LT}, G_{TT}	shear moduli in plane of fibers and normal to it, respectively
$\{H\}$	vector of stress resultant (or internal force) parameters
h	total thickness of laminate
$h_1, h_2, h_3, h_4, h_5, h_6, h_7$	wall thicknesses (see tables 2 and 3)

I_y, I_z, I_{yz}	second moments of cross section (moments and product of inertia) of one-dimensional-beam model
I_ω	principal second sectorial moment of cross section of one-dimensional-beam model
J	Saint-Venant torsion constant of cross section of one-dimensional-beam model
K	kinetic energy
$[\mathring{K}]$	generalized stiffness matrix for an individual element (see eqs. (3))
l	length of individual finite element
M_y, M_z, M_t	bending and twisting moments in one-dimensional-beam model
$M_1, M_2,$ M_{12}, M_{21}	bending stress resultants in two-dimensional model
$[M], [\mathring{M}]$	consistent and generalized mass matrices for an individual element (see eqs. (3))
N_1, N_2, N_{12}	extensional stress resultants in two-dimensional model
NL	total number of layers
N_x	axial force in one-dimensional-beam model
$[P], [Q]$	matrices associated with constraint condition and regularization term in the functional for one-dimensional-beam model
Q_y, Q_z	transverse shear forces in one-dimensional-beam model
Q_1, Q_2	transverse shear stress resultants in two-dimensional model
R	radius of curvature of centerline of frame (used in one-dimensional-beam model)
R_1	outer radius of curvature of frame (see fig. 1)
$[S]$	strain-displacement matrix for individual element
U^c	total complementary strain energy of frame
U_{tf}, U_w, U_{bf}	contributions of top flange, web, and bottom flange (including skin) to total complementary strain energy
U_1, U_2	complementary strain-energy components associated with in-plane and out-of-plane forces, respectively
U_3	complementary strain-energy component associated with forces neglected in one-dimensional-beam model
u, v, w	displacement components in coordinate directions for one-dimensional-beam model
u^0, v^0, w^0	axial and transverse displacements of one-dimensional-beam model at $y = z = 0$
u_1, u_2, w	displacement components of two-dimensional model in x_1, x_2, x_3 coordinate directions
u_1', u_2', w'	displacement components of two-dimensional model in x_1', x_2', x_3' coordinate directions
$\{X\}$	vector of nodal displacements
x, y, z	centroidal orthogonal coordinate system used for one-dimensional-beam model
x_1, x_2, x_3	local orthogonal coordinate system used in conjunction with two-dimensional model (for the web and each of the two flanges)
x_1', x_2', x_3'	global Cartesian coordinates used for two-dimensional model
$\{Z\}$	vector of element degrees of freedom
$\{\mathring{Z}\}$	particular solution (see eqs. (5) and (7))
$\gamma_{xy}, \gamma_{xz},$ $\gamma_{xy}^0, \gamma_{xz}^0$	transverse shear strains in one-dimensional-beam model (see eqs. (A2))
ε	penalty parameter
ε_x	extensional strain in one-dimensional-beam model
ε_x^0	extensional strain of centerline of one-dimensional-beam model
$\bar{\theta}$	angle that a typical cross section of frame makes with x_1', x_2' plane

θ^0	rate of twist of one-dimensional-beam model
$\kappa_y^0, \kappa_z^0, \kappa_t^0$	curvature changes and twist of one-dimensional-beam model
$\{\bar{\lambda}\}$	vector of Lagrange multiplier parameters
$\widehat{\lambda}$	Lagrange multiplier
λ_i	lamination and material parameters
ν_{LT}	major Poisson's ratio of individual layers
$\sigma_x, \sigma_{xy}, \sigma_{xz}$	normal and shearing stresses on cross section of beam
π, π_{HR}	functionals defined in equations (A7) and (A8)
ρ	mass density of material
ϕ_1, ϕ_2	rotation components of two-dimensional model referred to local coordinate system x_1, x_2
$\phi_1', \phi_2', \phi_3'$	rotation components of two-dimensional model referred to global coordinate system x_1', x_2', x_3'
$\phi_x^0, \phi_y^0, \phi_z^0$	rotation components in one-dimensional-beam model
Ψ^0	strain parameter in one-dimensional-beam model
ω	frequency of vibration
$\overline{\omega}$	sectorial coordinate (warping of cross section for a unit rate of twist)
∂	$\equiv d/dx$
1D	one-dimensional-beam model
2D	two-dimensional model
Subscript:	
s	shear center
Superscript:	
t	matrix transposition

Analysis

Computational Models

Two computational models are used for the thin-walled composite frames considered in the present study. In the first model, the flanges and web are modeled by using two-dimensional shell and plate finite elements. The second model is a finite-element discretization of the one-dimensional Vlasov type thin-walled-beam theory. Herein, the two models are referred to as two-dimensional (2D) and one-dimensional (1D) finite-element models, respectively.

Mathematical Formulation

Two-dimensional models. The analytical formulation for the two-dimensional models is based on the Sanders-Budiansky shell theory with the effects of transverse shear deformation, and laminated anisotropic material response included. A mixed formulation is used in which the fundamental unknowns consist of the generalized displacements and the stress resultants in the frame. (See fig. 2 for the sign convention.)

Bicubic shape functions are used to approximate each of the generalized displacements and stress resultants. There are 16 displacement nodes and 128 stress-resultant parameters in each element. The stress resultants are allowed to be discontinuous at interelement boundaries. The element characteristic arrays are obtained by using the two-field, Hellinger-Reissner, mixed-variational principle.

One-dimensional models. The analytical formulation for one-dimensional models is based on a form of the Vlasov thin-walled-beam theory with the effects of flexural-torsional coupling, transverse shear deformation, and rotary inertia included. The fundamental unknowns consist of seven internal forces and seven generalized displacements of the beam (see fig. 3 for the sign convention). The element characteristic arrays are obtained by using a modified form of the Hellinger-Reissner mixed variational principle. The modification consists of augmenting the functional of that principle by two terms: (1) the Lagrange multiplier associated with the constraint condition relating the rotation of the cross section and the twist degrees of freedom, and (2) a regularization term that is quadratic in the Lagrange multiplier. Only C^o continuity is required for the generalized displacements. Lagrangian interpolation functions are used for approximating each of the generalized displacements, internal forces, and Lagrange multiplier. The polynomial functions for the internal forces and the Lagrange multiplier are one degree lower than those of the generalized displacements. In the present study, quadratic polynomials are used in approximating the generalized displacements. Linear polynomials are used in approximating each of the internal forces and the Lagrange multiplier. The internal forces and the Lagrange multiplier are allowed

to be discontinuous at interelement boundaries. For each element, the total number of generalized displacement parameters is 21, the total number of internal force parameters is 14, and the total number of Lagrange multiplier parameters is 2. The fundamental equations of the thin-walled-beam theory used in the present study are given in Noor, Peters, and Min (1989) and are summarized in the appendix.

For quasi-isotropic laminated composites, numerical experiments to be described subsequently have demonstrated that reasonably accurate results can be obtained with the one-dimensional model when the laminated composite is replaced by an equivalent isotropic material with the following Young's and shear moduli:

$$E = A_{11}/h \tag{1}$$

$$G = A_{33}/h \tag{2}$$

where A_{11} and A_{33} are the extensional stiffness in the x-direction and the in-plane shear stiffness used in the classical lamination theory, and where h is the total wall thickness (of the flange or web). This approximation was adopted in the present study.

Finite-Element Equations

The finite-element equations for each individual element of the two-dimensional and one-dimensional models can be cast in the following compact form:

$$\left([\mathring{K}] - \omega^2[\mathring{M}]\right)\{Z\} = 0 \tag{3}$$

where $\{Z\}$ is the vector of the element degrees of freedom, ω is the frequency of vibration, and $[\mathring{K}]$ and $[\mathring{M}]$ are the generalized stiffness and mass matrices. The forms of $\{Z\}$, $[\mathring{K}]$, and $[\mathring{M}]$ are defined in the following table, where $\{H\}$, $\{X\}$, and $\{\bar{\lambda}\}$ are the vectors of stress-resultant (or internal force) parameters, nodal displacements, and Lagrange multiplier parameters, respectively; $[F]$ is the matrix of linear flexibility coefficients; $[S]$ is the strain displacement matrix; $[P]$ and $[Q]$ are matrices associated with the constraint condition and the regularization term in the functional, respectively; $[M]$ is the consistent mass matrix; ε is a penalty parameter associated with the regularization term; superscript t denotes transposition; and a dot $(\cdot)$ refers to a zero submatrix. The explicit form of the arrays in the following table is given in Noor and Andersen (1982) and Noor and Peters (1983) for the two-dimensional models and in Noor, Peters, and Min (1989) for the one-dimensional models:

Array	Two-dimensional models	One-dimensional models
$\{Z\}$	$\begin{Bmatrix} H \\ X \end{Bmatrix}$	$\begin{Bmatrix} H \\ X \\ \bar{\lambda} \end{Bmatrix}$
$[\mathring{K}]$	$\begin{bmatrix} -F & S \\ S^t & \cdot \end{bmatrix}$	$\begin{bmatrix} -F & S & \cdot \\ S^t & \cdot & Q \\ \cdot & Q^t & \frac{P}{\varepsilon} \end{bmatrix}$
$[\mathring{M}]$	$\begin{bmatrix} \cdot & \cdot \\ \cdot & M \end{bmatrix}$	$\begin{bmatrix} \cdot & \cdot & \cdot \\ \cdot & M & \cdot \\ \cdot & \cdot & \cdot \end{bmatrix}$

Sensitivity of Vibrational Response to Variations in Lamination and Material Parameters

The expressions for the sensitivity derivatives of the frequency and response vectors with respect to the lamination and material parameters λ_i of the composite frames are given by (Nelson 1976)

$$\frac{\partial\omega^2}{\partial\lambda_i} = \sum_{\text{Elements}} \{Z\}^t \left(\frac{\partial[\mathring{K}]}{\partial\lambda_i} - \omega^2\frac{\partial[\mathring{M}]}{\partial\lambda_i}\right)\{Z\} \tag{4}$$

and

$$\frac{\partial\{Z\}}{\partial\lambda_i} = \{\mathring{Z}\} + c_i\{Z\} \tag{5}$$

where $\{\mathring{Z}\}$ represents a particular solution of the equations

$$([\mathring{K}] - \omega^2[\mathring{M}])\frac{\partial\{Z\}}{\partial\lambda_i} = -\left(\frac{\partial[\mathring{K}]}{\partial\lambda_i} - \omega^2\frac{\partial[\mathring{M}]}{\partial\lambda_i} - \frac{\partial\omega^2}{\partial\lambda_i}[\mathring{M}]\right)\{Z\} \tag{6}$$

and c_i are multipliers given by

$$c_i = -\sum_{\text{Elements}} \left(\{\mathring{Z}\}^t[M]\{Z\} + \{Z\}^t\left[\frac{\partial M}{\partial\lambda_i}\right]\{Z\}\right) \tag{7}$$

In equations (4) to (7), the eigenvectors are assumed to be normalized with respect to $[\mathring{M}]$; that is,

$$\{Z\}^t[\mathring{M}]\{Z\} = 1 \tag{8}$$

The expressions for the total complementary strain energy of the frame U^c and its derivatives with

respect to λ_i are given by

$$U^c = \frac{1}{2} \sum_{\text{Elements}} \{H\}^t [F] \{H\} \tag{9}$$

and

$$\frac{\partial U^c}{\partial \lambda_i} = \sum_{\text{Elements}} \left(\frac{1}{2} \{H\}^t \frac{\partial [F]}{\partial \lambda_i} \{H\} + \left\{ \frac{\partial H}{\partial \lambda_i} \right\}^t [F] \{H\} \right) \tag{10}$$

For the purpose of obtaining analytic derivatives with respect to some of the lamination parameters, such as the fiber orientation angle of different layers, it is convenient to express $\frac{\partial [F]}{\partial \lambda_i}$ in terms of $\frac{\partial [F]^{-1}}{\partial \lambda_i}$ as follows:

$$\frac{\partial [F]}{\partial \lambda_i} = -[F] \frac{\partial [F]^{-1}}{\partial \lambda_i} [F] \tag{11}$$

The matrix $\frac{\partial [F]^{-1}}{\partial \lambda_i}$ is evaluated using the analytical derivatives of the material stiffness matrix of each laminate (flanges and web). The material stiffness matrix of the laminate is given in Jones (1975).

Experimental and Numerical Studies

Apparatus and Test Procedure

Specimens. Two specimens, an I-section and a J-section frame (fig. 4), were tested in the present study. Nominal dimensions of each cross section are given in figure 1. Weights of the frame sections were 3.181 lb and 4.085 lb for the I and J frames, respectively. The frame sections were made from AS4/5208 graphite-epoxy unidirectional tape laid up in a manner that resulted in essentially uniform stiffness properties in the circumferential direction (i.e., the stiffness coefficients are independent of $\bar{\theta}$). The material properties for the individual layers are given in figure 1. The laminate stacking sequence was $[\pm 45/0/90]_s$ for the I-section and $[\pm 45/0/90]_{2s}$ for the J-section. Each frame section was semicircular with a diameter of 72 in. Bonded to the outside flange of each frame was a 16-ply $[\pm 45/0/90]_{2s}$, quasi-isotropic skin made of the same material. The frame sections were constructed so that the skin would extend 0.5 in. beyond each side of the bottom flange of the frame. The nominal dimensions of the I- and J-section frames are given in figure 1, and the actual (measured) dimensions are given in tables 1 and 2.

Apparatus and procedure. Figure 5 is a schematic of the experimental setup, and figure 4 is a photograph of the setup and specimens. The ends of the frame sections were potted in a fixture that was bolted to a large steel-beam backstop. (See fig. 4.)

An air shaker, connected to an air compressor, was used to excite all test specimens. Excitation was both in plane (radially) and out of plane. For in-plane excitation, the shaker was positioned so that the pulses of air struck approximately normal to the surface of the skin. For out-of-plane excitation, a piece of Dow Chemical Co. Styrofoam was attached to the side of the frame by double-sided adhesive tape. Pulses of air struck the flat face of the Styrofoam normal to the face. The position of the air shaker was adjusted when the excitation was striking on a node.

A miniature accelerometer was attached at a fixed location to the frame sections with double-sided adhesive tape. Output from the accelerometer was amplified and displayed along the vertical axis of an oscilloscope. Natural modes were determined by tuning the excitation frequency of the air shaker to produce a maximum acceleration of the vertical deflection on the oscilloscope. Output also passed through a low-pass filter and was displayed as vibrational frequency on a frequency counter.

A hand-held velocity probe was moved along the frame to determine node locations and mode shapes. The output of the probe was displayed along the horizontal axis of the oscilloscope. The probe and accelerometer outputs combined to create a Lissajous pattern on the oscilloscope. A phase shift in the Lissajous pattern occurred when the velocity probe passed over a node.

The nodal locations were mapped manually during the vibration survey of the frames. Consequently, the only nodal lines monitored were those associated with gross in-plane and out-of-plane motions. Other nodal lines, associated with localized deformation patterns, were not surveyed. These localized deformations were noticeable in some of the higher vibration modes, with complex deformation patterns and/or strong coupling between in-plane and out-of-plane motions.

Finite-Element Grids

Two-dimensional models were generated for the actual frames (test specimens) described in the preceding section and for the corresponding frames with nominal dimensions. Herein, the frames with actual and nominal dimensions will be referred to as the actual and nominal frames, respectively. For the actual frames, spline interpolations were used to generate the wall thicknesses and coordinates of the nodal points. Isoparametric finite elements were used to approximate the variations in stiffness and geometry. The one-dimensional models considered herein

are for the frames with nominal dimensions. The grids used for both the one-dimensional and two-dimensional models are described subsequently.

Two-dimensional models. An 18 × 8 grid was used for modeling the whole I-section frame. In this grid, two elements were used to model each of the web, top flange, and bottom flange sections. The part of the skin adjacent to the bottom flange section was treated as part of the flange. One element was used to model each of the two parts of the skin section that extended beyond the bottom flange. (See fig. 1.) The middle surfaces of the top flange and the web were taken to be their reference surfaces. The middle surface of the combined bottom flange and skin was taken to be the reference surface.

An 18 × 7 grid was used for modeling the whole J-section frame. The distribution of the elements was similar to that for the I-section frame. Only one element was used to model the top flange section. (See fig. 1.)

Totally clamped and partially clamped support conditions were considered. For totally clamped supports, all six generalized displacements were restrained ($u_1' = u_2' = w' = \phi_1' = \phi_2' = \phi_3' = 0$). The partially clamped conditions were obtained from the totally clamped case by successively removing the restraints on one, as well as on combinations, of the displacement and rotation components.

One-dimensional models. A uniform grid of 24 elements was used in modeling each of the I-section and J-section frames. The principal sectorial properties of the cross section were evaluated with the Fortran program listed in Coyette 1987.

Identification of Modes and Estimation of Error in One-Dimensional-Model Predictions

The two-dimensional models can be used to identify the in-plane, out-of-plane, and coupled modes and to estimate the error in the predictions of the one-dimensional models. These objectives can be accomplished by decomposing the complementary strain energy U^c (eq. (9)) associated with each vibration mode into three components, U_1, U_2, and U_3 (see table 3). The first two components, U_1 and U_2, are associated with the in-plane and out-of-plane stress resultants, respectively. The third component, U_3, is associated with the stress resultants that are peculiar to two-dimensional plates and shells (not present in one-dimensional-beam models). The in-plane and out-of-plane modes correspond to the modes for which U_1/U^c and U_2/U^c are close to 1, respectively. The strongly coupled modes correspond to nearly equal values of U_1/U^c and U_2/U^c. The ratio U_3/U^c is indicative of the error in the one-dimensional-model predictions.

It is also useful to partition the total complementary strain energy associated with each mode into three components, U_{tf}, U_w, and U_{bf}; these components represent the contributions of the top flange, web, and bottom flange (including the skin).

Comparison of Experimental and Finite-Element Results

The results of the experimental and numerical studies are summarized in figures 6 to 10 and table 4 for the I-section frame, and in figures 11 to 15 and table 5 for the J-section frame. Figures 6(a) and 11(a) are bar charts for the experimental frequencies and the frequencies obtained by the two-dimensional finite-element model for the actual I-section and J-section frames, respectively. For the finite-element model, three cases are considered—totally clamped edges (with both translational and rotational restraints), partially clamped edges with ϕ_2' not restrained, and partially clamped edges with u_1' in the flanges and ϕ_2' not restrained.

The maximum and minimum values of the frequencies obtained by the two-dimensional finite-element model (corresponding to the totally clamped and partially clamped edges) are shown in figures 6(b) and 11(b), along with the experimental frequencies. (See also tables 4 and 5.) The experimental frequencies associated with modes 9 and 10 of the I-section frame, and with modes 9, 10, and 11 of the J-section frame, respectively, are close in frequency and have very close nodal locations. Henceforth these modes will be referred to collectively as mode 9. Also, the 12th mode of the I-section frame (table 4) was missed in the experimental survey, which is indicative of the difficulty of determining the high-frequency modes. The nodal locations of the succeeding experimental frequency for both the I- and J-section frames are close to those of the finite-element model. The fact that only one of the multiple experimental frequencies with close nodal locations is predicted by the finite-element model may be attributed to imperfections in lamination and material properties and/or to geometric nonlinearities that were not incorporated into the finite-element model. Figures 6(c) and 11(c) are bar charts for the frequencies obtained by two-dimensional models of the actual and nominal frames along with those of the one-dimensional model.

Figures 7 and 12 are bar charts of the two decompositions of the complementary strain energies, associated with the different vibration modes, described in the preceding section. The ordinates in figures 7(a) and 12(a) represent the ratios of U_1/U^c, U_2/U^c, and

U_3/U^c, and the ordinates in figures 7(b) and 12(b) represent the ratios of U_{tf}/U^c, U_w/U^c, and U_{bf}/U^c for each of the modes.

The mode shapes associated with the first 10 frequencies are shown in figures 8 and 13. Three views are shown for the deformations associated with each mode—side view, top view, and end view. Also shown are the nodal lines of the w' displacement on the top and bottom flanges. As can be seen in figures 8 and 13, the deformation patterns associated with higher modes are fairly complex. As mentioned previously, the only experimental nodal lines monitored are those associated with gross in-plane and gross out-of-plane motions. Generally, good agreement between the finite-element and experimental nodal lines is observed in these cases. Other nodal lines, associated with localized deformations, are shown only for the finite-element solutions.

The sensitivities of the vibration frequencies to the fiber orientation angles of the top flange, web, and bottom flange and skin are depicted in figures 9 and 14. The ordinates in figures 9 and 14 represent the sensitivity derivatives with respect to the indicated fiber angles. Each of the sensitivity derivatives is normalized by dividing it by the corresponding frequency of vibration. The sensitivities of the vibration frequencies to the material parameters E_L, E_T, G_{LT}, and G_{TT} are shown in figures 10 and 15. The ordinates in figures 10 and 15 represent the sensitivity derivatives with respect to the indicated elastic moduli. Each of the sensitivity derivatives is divided by the corresponding frequency and multiplied by the corresponding elastic modulus. The effects of boundary conditions on the frequencies obtained by the two-dimensional finite-element model are shown in tables 4 and 5.

An examination of the experimental and finite-element results (figs. 6 to 15 and tables 4 and 5) reveals the following:

1. Reasonably good correlation is observed between numerical simulation and experiment for the I-section frame (fig. 6(a)). The ratios of the first five experimental frequencies to the corresponding finite-element frequencies ranged from 0.90 to 1.00 (table 4). For the J-section frame, the correlation is not as good (fig. 11(a)). The corresponding ratios for the first five frequencies were from 0.86 to 1.01 (table 5).

2. Most of the experimental frequencies for the I-section frame and the J-section frame are between those for the totally and partially clamped supports (with both u_1' in the flanges and ϕ_2' not restrained), especially for the higher modes. For some of the modes, the experimental frequencies are closer to the partially clamped support case (e.g., modes 5, 7, 10, 12, and 13 (fig. 11(b))). For the I- and J-section frames, the finite-element model predicted only one of the multiple experimental modes with close nodal lines. The other experimental frequencies were between those for the totally and partially clamped supports (with both u_1' in the flanges and ϕ_2' not restrained (figs. 6(b) and 11(b))).

3. The lowest five frequencies obtained by the one-dimensional model are reasonably close to those obtained by the corresponding two-dimensional model, especially for the J-beam, where the errors in the predictions of the one-dimensional model were well below 10 percent. (See figs. 6(c) and 11(c).)

4. Identification of the modes as in plane or out of plane can best be accomplished by examining the energy components, U_1/U^c and U_2/U^c, associated with the in-plane and out-of-plane forces, respectively (figs. 7(a) and 12(a)). Also, the minimum error to be expected when using one-dimensional thin-walled beams can be estimated by computing the ratio of the energy associated with the forces neglected in thin-walled beams to the total energy U_3/U^c. (See figs. 7(a) and 12(a).)

5. The coupling between in-plane and out-of-plane deformations is more pronounced in the J-section frame than in the I-section frame. For example, the first 20 modes for the I-section frame had either U_1/U^c or $U_2/U^c \geq 0.75$. On the other hand, only modes 1 to 4, 6, 8, and 10 in the J-section frame had U_1/U^c or $U_2/U^c \geq 0.75$. For the higher modes, neither U_1/U^c nor U_2/U^c was close to 1. (See figs. 7(a) and 12(a).)

6. For the I-section frame, the contributions of the top and bottom flanges to the total energy associated with different modes far exceeded that of the web. The ratio of the strain energy in the web to the total strain energy was less than 0.20 for the first 10 modes (fig. 7(b)) and less than 0.28 for the succeeding 10 modes. For the J-section frame, the strain-energy ratio in the web approached 0.4 in some of the modes (fig. 12(b)).

7. For the I-section frame, the strain energy of the top flange is the dominant energy in the in-plane deformation modes, and the strain energy of the bottom flange (including the skin) dominates for the out-of-plane deformation modes. (See fig. 7(b).)

8. The vibrational response of both the I-section and J-section frames is very sensitive to restraining the u_1 displacements of the flanges (and skin). It is somewhat sensitive to the rotational restraint on ϕ_2'. (See tables 4 and 5.) However, it is less sensitive to restraining the displacement components u_2' and w' and the rotation ϕ_1'.

9. The vibrational response of the I-section frame and J-section frame is more sensitive to variations

in the 45° or −45° fiber angles than to variations in the 0° or 90° fiber angles. The variations in the 0° and 90° fibers of the web and the bottom flange have a noticeable effect on some of the modes, but their effect is generally less than that of the 45° and −45° fibers. (See figs. 9 and 14.) The vibrational response is also more sensitive to variations in the elastic moduli E_L and G_{LT} than to any of the other material coefficients. (See figs. 10 and 15.)

10. The sensitivity of the vibration frequencies with respect to variations in both E_L and G_{LT} is almost the same for all the modes. (See figs. 10 and 15.) This uniform sensitivity may be attributed to the quasi-isotropic lamination used for both the flanges and the web. It suggests the feasibility of replacing the quasi-isotropic composite, in the one-dimensional thin-walled-beam model, with an equivalent isotropic material, as was done in the present study.

Comments on Sources of Errors and Model Adjustment Techniques

Sources of Errors

The determination of natural frequencies and modes from vibration tests and numerical models involves numerous possible sources of discrepancies or errors that are related to mechanical and equipment limitations and to theoretical and physical assumptions. The errors in vibration tests include inexact equipment calibration, excessive noise, manufacturing variations, incorrect transducer locations, and operation in a region of nonlinearity of the response. Numerical modeling errors can be attributed to inaccuracies in estimated material properties and to insufficient modeling detail. In the present study, care was exercised in collecting and recording the vibration test data and in the selection of the numerical model. However, nominal material properties and lay-ups (fiber orientation of the different layers) were used in the numerical model. The sensitivity analysis helped identify the material and lamination parameters that need to be accurately determined.

Model Adjustment Techniques

In recent years, considerable efforts have been directed at improving and modifying the numerical model to obtain a better correlation with test results. These efforts started as trial-and-error approaches and evolved into systematic system identification and model adjustment techniques. Although these model adjustment techniques have not been used in the present study, the techniques are particularly useful for validating numerical models to be used in simulating transient dynamic response.

Most of the model adjustment techniques are based on using the experimental modal data (measured eigenvalues and eigenvectors) to update the stiffness and/or mass matrices of the structure (e.g., see Berman 1979; Chen 1979; Wei 1980; Berman and Wei 1981; Baruch 1982; Grossman 1982; Berman and Nagy 1983; Jensen and Crawley 1984; Kabe 1985; and Arruda and dos Santos 1989) and the two monographs (Ewins 1986 and Martinez and Miller 1985). In some of the recent techniques, the sensitivity derivatives with respect to the physical parameters of the numerical model are used in conjunction with optimization algorithms to obtain corrected (or adjusted) values of the physical parameters.

Conclusions

A detailed study is made of the effects of variations in lamination and material parameters of thin-walled composite frames on their vibrational characteristics. The structures considered are semicircular thin-walled frames with I- and J-section frames. The flanges, web, and skin of the stiffeners have quasi-isotropic laminations and the fiber orientation is made up of combinations of ±45°, 0°, and 90° layers. Two computational models are used for predicting the vibrational characteristics. In the first model, the flanges and webs of the stiffeners are modeled by using two-dimensional shell (and plate) finite elements. The second model is a finite-element discretization of the one-dimensional Vlasov-type thin-walled-beam theory. A mixed formulation is used with the fundamental unknowns consisting of both the generalized displacements and stress resultants (or internal forces) in the frame. The frequencies and modes predicted by the computational models are compared with those obtained from experiments. A detailed study is made of the sensitivity of the vibration response to variations in the fiber orientation, material properties of the individual layers, and boundary conditions. On the basis of this study, the following conclusions are justified:

1. For some of the higher vibration modes, the experimental frequencies for thin-walled frames are generally between those for the totally and partially clamped supports.

2. Identification of the modes as in plane or out of plane can best be accomplished by examining the energy components associated with the in-plane and out-of-plane forces. Also, the minimum error to be expected when using one-dimensional thin-walled beams can be estimated by computing the ratio of the energy associated with the forces neglected in thin-walled beams to the total energy.

3. For quasi-isotropic composite frames, the vibration frequencies, associated with the lower modes, can be accurately predicted by an isotropic one-dimensional-beam model (with effective elastic moduli). The accuracy of predictions is dependent on the cross-sectional distortions during the beam deformations. As the cross-sectional distortions increase, the degradation of accuracy becomes more pronounced.

4. The vibrational response of thin-walled semicircular frames is very sensitive to restraining the u_1' displacement component of the flanges along the length of the frame. It is somewhat sensitive to the restraint on the associated rotation component. However, it is less sensitive to restraining the other displacement and rotation components.

5. The vibrational response of thin-walled composite frames with quasi-isotropic laminations is more sensitive to variations in the $+45°$ or $-45°$ fiber angles than to variations in the $0°$ or $90°$ fiber angles. Variations in the $0°$ and $90°$ fibers of the web and the bottom flange have a noticeable effect on some of the modes, but their effect is generally less than that of the $45°$ and $-45°$ fibers. The vibrational response is also more sensitive to variations in the material coefficients E_L and G_{LT} than to all other coefficients.

6. The sensitivity of the vibration frequencies with respect to variations in the elastic moduli E_L and G_{LT} is almost the same for all the modes because of the quasi-isotropic lamination used for both the flanges and the web. It suggests the feasibility of replacing the quasi-isotropic composite with an equivalent isotropic material in the one-dimensional thin-walled-beam analysis, as was done in the present study.

NASA Langley Research Center
Hampton, VA 23665-5225
September 4, 1990

Appendix

Fundamental Equations of Thin-Walled-Beam Theory Used in Present Study

The fundamental equations of the linear, Vlasov-type theory of curved thin-walled beams are given in this appendix. A right-handed orthogonal coordinate system is used with the x-axis passing through the centroids of the cross sections. (See fig. 3.) The beam is assumed to be curved in one direction only (in the xz-plane).

Displacement Assumptions

Based on the assumption that the projection of each cross section on a plane normal to the initial centroidal axes does not distort during deformation, the displacement field in the plane of the cross section (yz-plane) is represented by

$$\begin{Bmatrix} u(x,y,z) \\ v(x,y,z) \\ w(x,y,z) \end{Bmatrix} = \begin{Bmatrix} u^0 \\ v^0 \\ w^0 \end{Bmatrix} + \begin{bmatrix} \cdot & z & -y \\ -z & \cdot & \cdot \\ y & \cdot & \cdot \end{bmatrix} \begin{Bmatrix} \phi_x^0 \\ \phi_y^0 \\ \phi_z^0 \end{Bmatrix} - \begin{Bmatrix} \overline{\omega} \\ \cdot \\ \cdot \end{Bmatrix} \theta^0 \tag{A1}$$

where u^0, v^0, and w^0 are the axial and transverse displacement components at $y = z = 0$; ϕ_x^0, ϕ_y^0, and ϕ_z^0 are the rotation components about the coordinate axes; θ^0 is the rate of twist of the beam; and $\overline{\omega}$ is the sectorial coordinate (warping of the cross section for a unit rate of twist). The seven generalized displacement parameters u^0, v^0, w^0, ϕ_x^0, ϕ_y^0, ϕ_z^0, and θ^0 are functions of x only.

Strain Assumptions

The following expressions are used for the three nonzero components of the strain field in the plane of the cross section:

$$\left.\begin{aligned} \varepsilon_x &= \varepsilon_x^0 - y\kappa_y^0 + z\kappa_z^0 - \overline{\omega}\Psi^0 \\ \gamma_{xy} &= \gamma_{xy}^0 - z\kappa_t^0 \\ \gamma_{xz} &= \gamma_{xz}^0 + y\kappa_t^0 \end{aligned}\right\} \tag{A2}$$

where ε_x^0 is the extensional strain of the centerline, κ_y^0 and κ_z^0 are the curvature changes in the y- and z-directions, κ_t^0 is the twist, and γ_{xy}^0 and γ_{xz}^0 are the transverse shear strains. The strain parameters ε_x^0, κ_y^0, κ_z^0, γ_{xz}^0, γ_{xy}^0, κ_t^0 and Ψ^0 are functions of x only and can be expressed in terms of the displacement and rotation components as follows:

$$\left.\begin{aligned} \varepsilon_x^0 &= \partial u^0 + \frac{w^0}{R} \\ \kappa_y^0 &= \partial\phi_z^0 + \frac{\phi_x^0}{R} \\ \kappa_z^0 &= \partial\phi_y^0 \\ \gamma_{xy}^0 &= \partial v^0 - \phi_z^0 \\ \gamma_{xz}^0 &= -\frac{u^0}{R} + \partial w^0 + \phi_y^0 \\ \kappa_t^0 &= \partial\phi_x^0 + \frac{\phi_z^0}{R} \\ \Psi^0 &= \partial\theta^0 \end{aligned}\right\} \tag{A3}$$

where $\partial \equiv d/dx$ and R is the radius of curvature of the centerline of the beam. Also, the following constraint condition is used to relate θ^0 and ϕ_x^0:

$$\partial\phi_x^0 - \theta^0 = 0 \tag{A4}$$

Constitutive Relations

The relations betwen the internal forces and the strain components are given by

$$\begin{Bmatrix} N_x \\ M_z \\ M_y \\ B_\omega \end{Bmatrix} = \int_A \sigma_x \begin{Bmatrix} 1 \\ -y \\ z \\ \overline{\omega} \end{Bmatrix} dA = E \begin{bmatrix} A & \cdot & \cdot & \cdot \\ & I_z & -I_{yz} & \cdot \\ & & I_y & \cdot \\ \text{Symm} & & & I_\omega \end{bmatrix} \begin{Bmatrix} \varepsilon_x^0 \\ \kappa_y^0 \\ \kappa_z^0 \\ \Psi^0 \end{Bmatrix} \tag{A5}$$

and

$$\begin{Bmatrix} Q_y \\ Q_z \\ M_t \end{Bmatrix} = \int_A \begin{bmatrix} 1 & \cdot \\ \cdot & 1 \\ -z & y \end{bmatrix} \begin{Bmatrix} \sigma_{xy} \\ \sigma_{xz} \end{Bmatrix} dA = G \begin{bmatrix} A_y & \cdot & \cdot \\ \cdot & A_z & \cdot \\ \cdot & \cdot & J \end{bmatrix} \begin{Bmatrix} \gamma_{xy}^0 \\ \gamma_{xz}^0 \\ \kappa_t^0 \end{Bmatrix} \tag{A6}$$

where A is the cross-sectional area; I_y, I_z, and I_{yz} are the second moments of the cross section (moments and product of inertia); J is the Saint-Venant torsion constant; I_ω is the principal second sectorial moment of the cross section (sectorial moment of inertia); E and G are the effective Young's and shear moduli of the material; N_x is the axial force; M_y and M_z are the bending moments; B_ω is the bimoment; Q_y and Q_z are the transverse shearing forces; and M_t is the twisting moment. The definition of the sectorial properties of the cross section is given in Vlasov (1961), Zbirohowski-Kościa (1967), and Gjelsvik (1981).

Variational Functional

The functional used in the element development is given by

$$\pi = \pi_{HR} + \int_0^l \widehat{\lambda}(\partial\phi_x^0 - \theta^0)\,dx - \frac{1}{2\varepsilon}\int_0^l (\widehat{\lambda})^2\,dx \quad \text{(A7)}$$

where $\widehat{\lambda}$ is the Lagrange multiplier, ε is a penalty parameter, l is the length of the element, and π_{HR} is the functional of the Hellinger-Reissner mixed variational principle. The expression for π_{HR} is

$$\pi_{HR} = \int_0^l (V - U^c + K)\,dx \quad \text{(A8)}$$

where

$$V = \begin{Bmatrix} N_x \\ M_z \\ M_y \\ B_\omega \end{Bmatrix}^t \begin{Bmatrix} \varepsilon_x^0 \\ \kappa_y^0 \\ \kappa_z^0 \\ \Psi^0 \end{Bmatrix} + \begin{Bmatrix} Q_y \\ Q_z \\ M_t \end{Bmatrix}^t \begin{Bmatrix} \gamma_{xy}^0 \\ \gamma_{xz}^0 \\ \kappa_t^0 \end{Bmatrix} \quad \text{(A9)}$$

$$U^c = \frac{1}{2E}\begin{Bmatrix} N_x \\ M_z \\ M_y \\ B_\omega \end{Bmatrix}^t \begin{bmatrix} A & \cdot & \cdot & \cdot \\ & I_z & -I_{yz} & \cdot \\ & & I_y & \cdot \\ & \text{Symm} & & I_\omega \end{bmatrix}^{-1} \begin{Bmatrix} N_x \\ M_z \\ M_y \\ B_\omega \end{Bmatrix} + \frac{1}{2G}\begin{Bmatrix} Q_y \\ Q_z \\ M_t \end{Bmatrix}^t \begin{bmatrix} \frac{1}{A_y} & \cdot & \cdot \\ & \frac{1}{A_z} & \cdot \\ \text{Symm} & & \frac{1}{J} \end{bmatrix} \begin{Bmatrix} Q_y \\ Q_z \\ M_t \end{Bmatrix} \quad \text{(A10)}$$

$$K = \frac{\rho}{2}\omega^2\Big\{A\left[(u^0)^2 + (v^0)^2 + (w^0)^2\right] + (I_y + I_z)(\phi_x^0)^2 + I_y(\phi_y^0)^2 + I_z(\phi_z^0)^2 - 2I_{yz}\phi_y^0\phi_z^0 + I_\omega(\theta^0)^2\Big\} \quad \text{(A11)}$$

where ρ is the mass density of the material. In equations (A5) to (A11), y and z are centroidal coordinates. (See fig. 3.) A Fortran program for evaluating the principal sectorial properties is listed by Coyette (1987).

References

Ali, S. A.: Stability of Bending-Torsional Vibrations of Curved Thin-Walled Beams. *J. Sound & Vibration,* vol. 95, no. 3, Aug. 1984, pp. 341–350.

Arruda, José Roberto de F.; and dos Santos, José Maria C.: Model Adjusting of Structures With Mechanical Joints Using Modal Synthesis. *7th International Modal Analysis Conference, Vol. II,* Union College and Society for Experimental Mechanics, Inc., c.1989, pp. 850–856.

Bank, L. C.; and Kao, C. H.: The Influence of Geometric and Material Design Variables on the Free Vibration of Thin-Walled Composite Material Beams. *J. Vib., Acoust., Stress, & Reliab. Des.,* vol. 111, July 1989, no. 3, pp. 290–297.

Baruch, Menahem: Optimal Correction of Mass and Stiffness Matrices Using Measured Modes. *AIAA J.,* vol. 20, no. 11, Nov. 1982, pp. 1623–1626.

Berman, A.; and Nagy, E. J.: Improvement of a Large Analytical Model Using Test Data. *AIAA J.,* vol. 21, no. 8, Aug. 1983, pp. 1168–1173.

Berman, Alex: Mass Matrix Correction Using an Incomplete Set of Measured Modes. *AIAA J.,* vol. 17, no. 10, Oct. 1979, pp. 1147–1148.

Berman, Alex; and Wei, Fu Shang: *Automated Dynamic Analytical Model Improvement.* NASA CR-3452, 1981.

Bishop, R. E. D.; Cannon, S. M.; and Miao, S.: On Coupled Bending and Torsional Vibration of Uniform Beams. *J. Sound & Vibration,* vol. 131, no. 3, June 1989, pp. 457–464.

Boitnott, Richard L.; and Fasanella, Edwin L.: Impact Evaluation of Composite Floor Sections. SAE Paper 891018, Apr. 1989.

Boitnott, Richard L.; Fasanella, Edwin L.; Calton, Lisa E.; and Carden, Huey D.: Impact Response of Composite Fuselage Frames. SAE Paper 871009, Apr. 1987.

Chandra, Ramesh; Ngo, Hieu; and Chopra, Inderjit: Experimental Study of Thin-Walled Composite Beams. Presented at National Technical Specialists' Meeting on Advanced Rotorcraft Structures (Williamsburg, Va.), American Helicopter Soc., Inc., Oct. 1988.

Chen, Jay C.; and Garba, John A.: Matrix Perturbation for Analytical Model Improvement. AIAA Paper No. 79-0831, Apr. 1979.

Collins, J. Scott; and Johnson, Eric R.: *Static and Free-Vibrational Response of Semi-Circular Graphite-Epoxy Frames With Thin-Walled Open Sections.* NASA CR-186097, 1989.

Coyette, J. P.: An Improved Subroutine for the Estimation of Torsional Properties of Thin Walled Open Cross-Sections. *Eng. Comput.,* vol. 4, no. 3, Sept. 1987, pp. 240–242.

Ewins, D. J.: Modal Testing: *Theory and Practice.* Research Studies Press, Ltd., c.1986.

Falco, Marzio; and Gasparetto, Michelle: Flexural-Torsional Vibrations of Thin-Walled Beams. *Meccanica,* vol. 8, no. 3, Sept. 1973, pp. 181–189.

Gjelsvik, Atle: *The Theory of Thin Walled Bars.* John Wiley & Sons, Inc., c.1981.

Grossman, Daniel T.: An Automated Technique for Improving Modal Test/Analysis Correlation. *A Collection of Technical Papers, Part 2: Structural Dynamics and Design Engineering—AIAA/ASME/ASCE/AHS 23rd Structures, Structural Dynamics and Materials Conference,* May 1982, pp. 68–76. (Available as AIAA-82-0640.)

Gupta, R. K.; Venkatesh, A.; and Rao, K. P.: Finite Element Analysis of Laminated Anisotropic Thin-Walled Open-Section Beams. *Compos. Struct.,* vol. 3, no. 1, 1985, pp. 19–31.

Hasan, S. Ali; and Barr, A. D. S.: Linear Vibration of Thin-Walled Beams of Equal Angle-Section. *J. Sound & Vibration,* vol. 32, no. 1, Jan. 1974, pp. 3–23.

Jensen, D. W.; and Crawley, E. F.: Frequency Determination Techniques for Cantilevered Plates With Bending-Torsion Coupling. *AIAA J.,* vol. 22, no. 3, Mar. 1984, pp. 415–420.

Jones, Robert M.: *Mechanics of Composite Materials.* McGraw-Hill Book Co., c.1975.

Kabe, Alvar M.: Stiffness Matrix Adjustment Using Mode Data. *AIAA J.,* vol. 23, no. 9, Sept. 1985, pp. 1431–1436.

Martinez, David R.; and Miller, A. Keith, eds.: Combined Experimental/Analytical Modeling of Dynamic Structural Systems. America Soc. of Mechanical Engineers, AMD-Vol. 67, c.1985.

Narayanan, S.; Verma, J. P.; and Mallik, A. K.: Free Vibration of Thin-Walled Open Section Beams With Unconstrained Damping Treatment. *J. Appl. Mech.,* vol. 48, no. 1, Mar. 1981, pp. 169–173.

Nelson, Richard B.: Simplified Calculation of Eigenvector Derivatives. *AIAA J.,* vol. 14, no. 9, Sept. 1976, pp. 1201–1205.

Noor, Ahmed K.; and Andersen, C. M.: Mixed Models and Reduced/Selective Integration Displacement Models for Nonlinear Shell Analysis. *Int. J. Numer. Methods Eng.,* vol. 18, no. 10, Oct. 1982, pp. 1429–1454.

Noor, Ahmed K.; and Peters, Jeanne M.: Mixed Models and Reduced Selective Integration Displacement Models for Vibration Analysis of Shells. *Hybrid and Mixed Finite Element Methods,* S. N. Atluri, R. H. Gallagher, and O. C. Zienkiewicz, eds., John Wiley & Sons Ltd., c.1983, pp. 537–564.

Noor, Ahmed K.; Peters, Jeanne M.; and Min, Byung-Jin: *Mixed Finite Element Models for Free Vibrations of Thin-Walled Beams.* NASA TP-2868, 1989.

Nowinski, J. L.: Theory of Thin-Walled Bars. *Applied Mechanics Surveys,* H. Norman Abramson, Harold Liebowitz, John M. Crowley, and Stephen Juhasz, eds., Spartan Books, 1966, pp. 325–338.

Panovko, Ya. G.; and Beilin, E. A.: Thin-Walled Beams and Systems Consisting of Thin-Walled Beams. *Structural Mechanics in the USSR—1917-1967,* I. M. Rabinovich, ed., Moskow Publ. House, 1969, pp. 75–98 (in Russian).

Potiron, A.; Gay, D.; Czekajski, C.; and Laroze, S.: Limitation of Simplified Hypotheses for the Prediction of Torsional Oscillations for Thin-Walled Beams. *J. Vib., Acoust., Stress, & Reliab. Des.,* vol. 107, no. 1, Jan. 1985, pp. 117–122.

Rao, C. Kameswara: Nonlinear Torsional Vibrations of Thin-Walled Beams of Open Section. *J. Appl. Mech.,* vol. 42, no. 1, Mar. 1975, pp. 240–242.

Rehfield, Lawrence W.; Atilgan, Ali R.; and Hodges, Dewey H.: Nonclassical Behavior of Thin-Walled Composite Beams With Closed Cross Sections. *J. American Helicopter Soc.*, vol. 35, no. 2, Apr. 1990, pp. 42–50.

Rückschloss, Ján; and Tesár, Alexander: Transfer Matrix Formulation for Solution of Torsion-Bending Vibration of Beams With Thinwalled Cross Sections. *ACTA TECHNICA ČSAV.* Vol. 5, no. 30, 1985.

Stemple, Alan D.; and Lee, Sung W.: Finite-Element Model for Composite Beams With Arbitrary Cross-Sectional Warping. *AIAA J.*, vol. 26, no. 12, Dec. 1988, pp. 1512–1520.

Teh, K. K.; and Huang, C. C.: The Effects of Fibre Orientation on Free Vibrations of Composite Beams. *J. Sound & Vibration,* vol. 69, no. 2, Mar. 1980, pp. 327–337.

Vasilenko, N. V.; and Trivailo, P. M.: Vibrations of Thin-Walled Rods With Open Profile of Material With Nonlinear Hysteresis. *Strength of Materials,* vol. 11, no. 11, July 1980, pp. 1279–1285.

Vermisyan, G. B.; and Galin, L. A.: Kruchenie Vyazko-Uprugogo Prizmaticheskogo Sterzhnya Pri Deictvii Vibratsionnoi Nagruzki. (Torsion of a Viscoelastic Prismatic Bar Acted Upon by a Vibrational Load.) *Izv. Akad. Nauk SSSR, Mech. Tverd. Tela.*, no. 5, Sept.–Oct. 1972, pp. 130–138.

Vlasov, V. Z. (Y. Schechtman, transl.): *Thin-Walled Elastic Beams.* Israel Program for Scientific Translations, 1961.

Wei, Fu-Shang: Stiffness Matrix Correction From Incomplete Test Data. *AIAA J.*, vol. 18, no. 10, Oct. 1980, pp. 1274–1275.

Wekezer, Jerzy W.: Free Vibrations of Thin-Walled Bars With Open Cross Sections. *J. Eng. Mech.*, vol. 113, no. 10, Oct. 1987, pp. 1441–1453.

Zbirohowski-Kościa, K.: *Thin Walled Beams—From Theory to Practice.* Crosby Lockwood & Son Ltd., 1967.

Table 1. Measured Thicknesses and Dimensions for I-Section Frame

$\bar{\theta}$, deg	h_1, in.	h_2, in.	h_3, in.	h_4, in.	h_5, in.	h_6, in.	h_7, in.	b_1, in.	b_2, in.	b_3, in.	b_4, in.	d_1, in.	d_2, in.
2	0.046	0.042	0.051	0.133	0.139	0.089	0.092	0.712	0.635	1.790	1.625	0.785	0.770
10	.041	.042	.046	.119	.125	.078	.086	.800	.633	1.795	1.670	.785	.785
20	.042	.043	.039	.127	.130	.084	.092	.800	.653	1.775	1.670	.800	.800
30	.041	.043	.041	.127	.126	.085	.091	.773	.680	1.780	1.680	.800	.810
40	.043	.044	.041	.121	.119	.080	.082	.775	.685	1.780	1.687	.815	.810
50	.045	.046	.046	.120	.116	.081	.081	.780	.675	1.770	1.685	.820	.810
60	.044	.045	.049	.124	.127	.085	.088	.795	.685	1.790	1.690	.820	.815
70	.043	.044	.055	.124	.131	.080	.093	.825	.680	1.775	1.680	.825	.810
80	.045	.044	.056	.125	.122	.085	.086	.825	.650	1.767	1.687	.815	.810
90	.051	.049	.050	.128	.129	.088	.091	.850	.645	1.780	1.660	.828	.790
100	.046	.045	.040	.119	.118	.083	.080	.830	.645	1.800	1.675	.812	.800
110	.045	.047	.039	.121	.122	.081	.081	.840	.635	1.790	1.690	.810	.790
120	.044	.047	.040	.118	.120	.083	.079	.800	.670	1.770	1.687	.810	.780
130	.045	.045	.041	.118	.122	.083	.078	.755	.690	1.765	1.705	.810	.790
140	.045	.044	.042	.120	.124	.082	.079	.730	.725	1.770	1.675	.805	.795
150	.044	.043	.041	.120	.120	.085	.079	.730	.708	1.785	1.670	.805	.785
160	.043	.043	.040	.123	.125	.086	.082	.710	.712	1.810	1.655	.800	.808
170	.043	.042	.052	.120	.117	.085	.077	.700	.728	1.795	1.655	.807	.785
178	.042	.044	.048	.136	.141	.093	.096	.692	.700	1.810	1.650	.800	.785

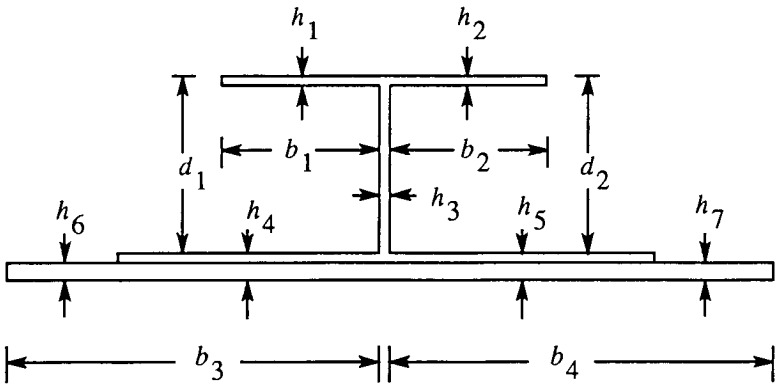

Table 2. Measured Thicknesses and Dimensions for J-Section Frame

$\bar{\theta}$, deg	h_1, in.	h_2, in.	h_3, in.	h_4, in.	h_5, in.	h_6, in.	b, in.	b_1, in.	b_2, in.	b_3, in.	d, in.
0	0.094	0.087	0.175	0.174	0.090	0.090	3.518	0.779	1.166	1.260	0.729
10	.095	.086	.168	.165	.091	.084	3.526	.784	1.191	1.240	.742
20	.094	.082	.168	.174	.087	.085	3.522	.754	1.299	1.239	.755
30	.086	.084	.166	.165	.086	.085	3.520	.724	1.289	1.264	.758
40	.087	.081	.165	.165	.086	.082	3.530	.722	1.266	1.215	.756
50	.086	.082	.168	.168	.091	.084	3.502	.728	1.272	1.217	.766
60	.091	.085	.162	.166	.084	.081	3.507	.721	1.250	1.183	.773
70	.090	.088	.167	.168	.086	.084	3.510	.735	1.258	1.257	.776
80	.090	.087	.165	.165	.085	.079	3.491	.739	1.236	1.241	.781
90	.090	.087	.178	.174	.091	.086	3.457	.750	1.281	1.240	.770
100	.100	.081	.172	.167	.085	.087	3.464	.768	1.308	1.277	.782
110	.090	.081	.167	.178	.085	.095	3.473	.753	1.273	1.303	.759
120	.090	.082	.167	.168	.085	.088	3.472	.767	1.244	1.263	.747
130	.090	.083	.173	.161	.086	.083	3.460	.762	1.256	1.253	.757
140	.088	.084	.175	.165	.088	.083	3.473	.761	1.254	1.250	.738
150	.087	.082	.168	.171	.085	.086	3.480	.750	1.253	1.260	.743
160	.093	.081	.174	.174	.087	.087	3.472	.776	1.238	1.283	.758
170	.086	.085	.173	.165	.088	.086	3.527	.715	1.231	1.283	.731
180	.091	.091	.185	.171	.093	.087	3.476	.664	1.220	1.282	.716

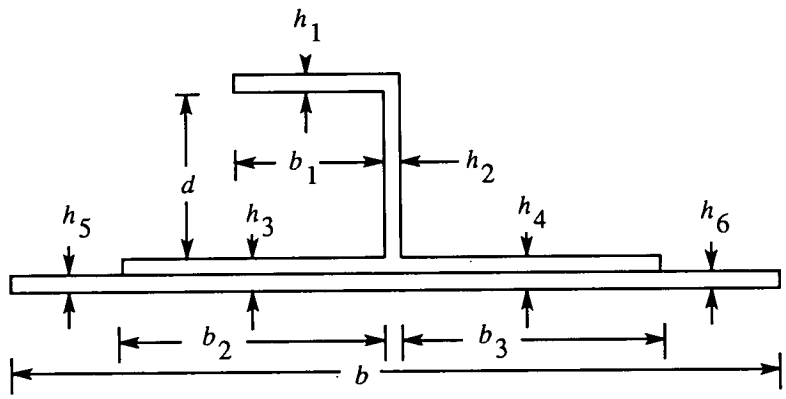

Table 3. Decomposition of Total Complementary Strain Energy Into Components

$$[U^c = U_1 + U_2 + U_3]$$

Energy components	Associated stress resultants (see fig. 2)		Comments
	Web	Flanges and skin	
U_1	$N_1,\ N_{12}$	$N_1,\ M_1, Q_1$	In-plane response quantities
U_2	$M_1,\ M_{12},\ Q_1$	$N_{12},\ M_{12}$	Out-of-plane response quantities
U_3	$N_2,\ M_2,\ Q_2$	$N_2,\ M_2,\ Q_2$	Response quantities neglected in one-dimensional model

Table 4. Effect of Boundary Conditions on Frequencies Obtained by Two-Dimensional Finite-Element Model for I-Section Frame

[Numbers in parentheses refer to ratios of partially clamped to totally clamped model frequencies]

Mode	Frequencies of totally clamped model, Hz	Frequencies of partially clamped model (with the following generalized displacements unrestrained), Hz				Experimental frequencies, Hz
		ϕ_2'	ϕ_2' and ϕ_3'	u_1' in flanges	u_1' in flanges and ϕ_2'	
1	9.201	9.001 (0.978)	9.001 (0.978)	6.788 (0.738)	6.632 (0.721)	9.2
2	31.86	31.06 (0.975)	31.06 (0.975)	18.11 (0.568)	17.87 (0.561)	29.7
3	37.52	37.37 (0.996)	37.37 (0.996)	34.17 (0.911)	33.36 (0.889)	35.9
4	73.85	71.82 (0.973)	71.81 (0.972)	38.09 (0.516)	37.69 (0.510)	66.6
5	81.34	81.03 (0.996)	81.03 (0.996)	74.30 (0.913)	73.44 (0.903)	78.1
6	133.9	130.1 (0.972)	130.1 (0.972)	75.56 (0.564)	74.14 (0.554)	119.0
7	149.2	148.6 (0.996)	148.6 (0.996)	129.6 (0.869)	128.1 (0.858)	145.0
8	203.3	198.1 (0.974)	198.1 (0.974)	139.8 (0.688)	137.4 (0.676)	193.0
9	226.5	225.6 (0.996)	225.6 (0.996)	199.3 (0.880)	196.9 (0.870)	216.0 223.0
10	281.9	275.2 (0.976)	275.2 (0.976)	214.2 (0.760)	210.9 (0.748)	260.0
11	320.6	319.3 (0.996)	319.3 (0.996)	268.0 (0.836)	264.9 (0.826)	309.0
12	349.8	342.3 (0.979)	342.3 (0.979)	305.1 (0.872)	300.7 (0.860)	(Missed)
13	419.1	412.6 (0.985)	412.6 (0.985)	343.0 (0.819)	339.0 (0.809)	401.0

Table 5. Effect of Boundary Conditions on Frequencies Obtained by Two-Dimensional Finite-Element Model for J-Section Frame

[Numbers in parentheses refer to ratios of partially clamped to totally clamped model frequencies]

Mode	Frequencies of totally clamped model, Hz	Frequencies of partially clamped model (with the following generalized displacements unrestrained), Hz				Experimental frequencies, Hz
		ϕ_2'	ϕ_2' and ϕ_3'	u_1' in flanges	u_1' in flanges and ϕ_2'	
1	11.53	11.24 (0.975)	11.24 (0.975)	8.488 (0.736)	8.408 (0.729)	11.6
2	36.87	36.64 (0.994)	36.64 (0.994)	22.41 (0.608)	22.37 (0.607)	32.1
3	39.81	38.80 (0.975)	38.79 (0.974)	32.77 (0.823)	32.18 (0.808)	37.0
4	79.22	78.99 (0.997)	78.99 (0.997)	48.32 (0.610)	47.94 (0.605)	69.0
5	91.41	88.81 (0.972)	88.78 (0.971)	72.64 (0.795)	71.68 (0.784)	79.0
6	143.9	143.5 (0.997)	143.5 (0.997)	96.58 (0.671)	95.35 (0.663)	126.0
7	168.1	163.6 (0.973)	163.5 (0.973)	134.4 (0.800)	132.9 (0.790)	145.0
8	214.1	213.4 (0.997)	213.4 (0.997)	167.2 (0.781)	165.0 (0.777)	191.0
9	263.0	256.9 (0.977)	256.8 (0.976)	206.5 (0.785)	204.3 (0.770)	221.0 229.0 247.0
10	297.6	296.2 (0.995)	296.2 (0.995)	251.5 (0.845)	248.3 (0.834)	266.0
11	368.2	361.2 (0.981)	361.1 (0.981)	298.7 (0.811)	295.5 (0.803)	339.0
12	382.8	380.3 (0.993)	380.3 (0.993)	336.7 (0.880)	332.8 (0.869)	347.0
13	468.2	462.0 (0.987)	461.9 (0.987)	402.4 (0.859)	398.0 (0.850)	403.0

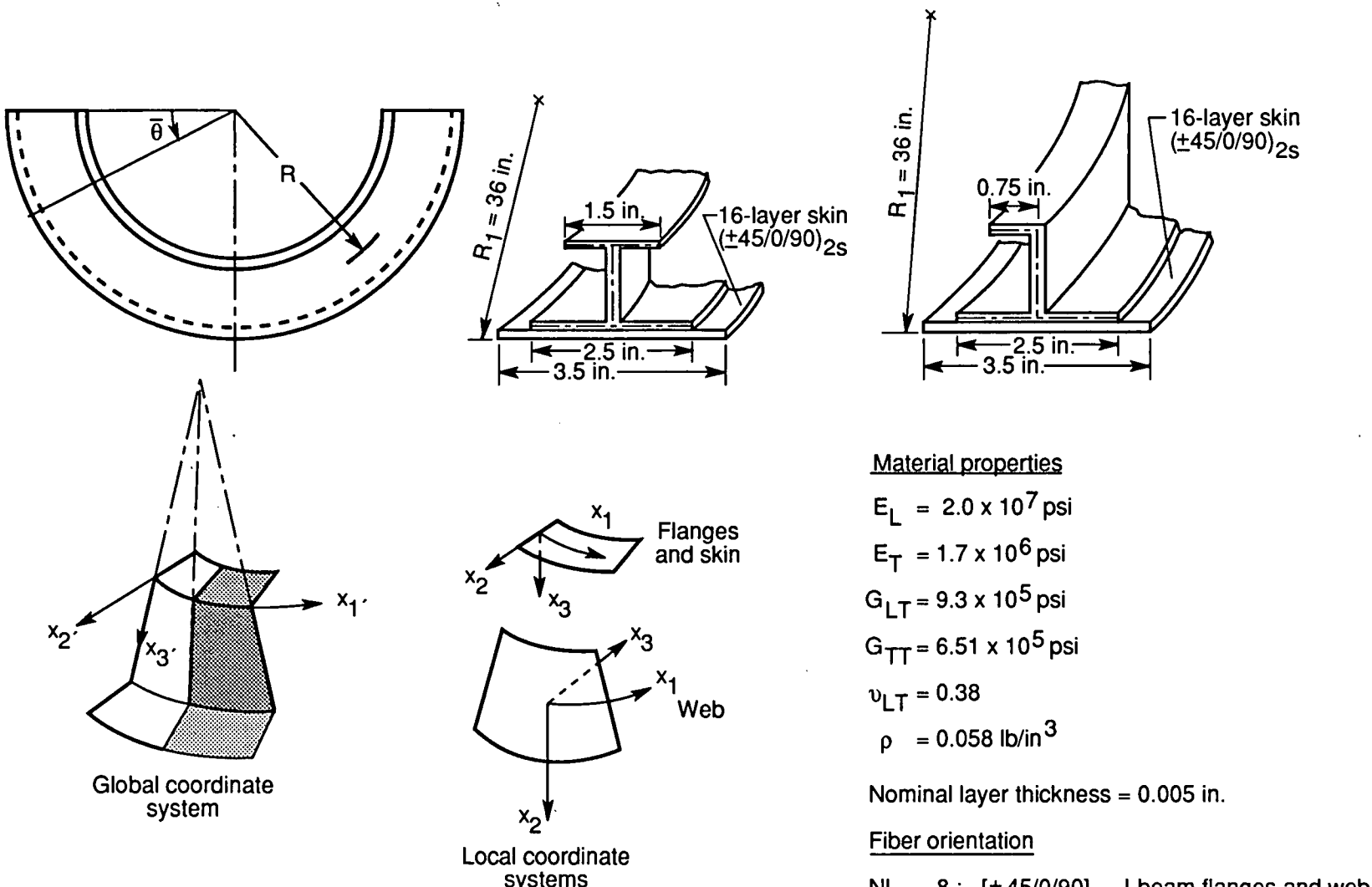

Figure 1. Thin-walled composite frames and coordinate systems used in present study.

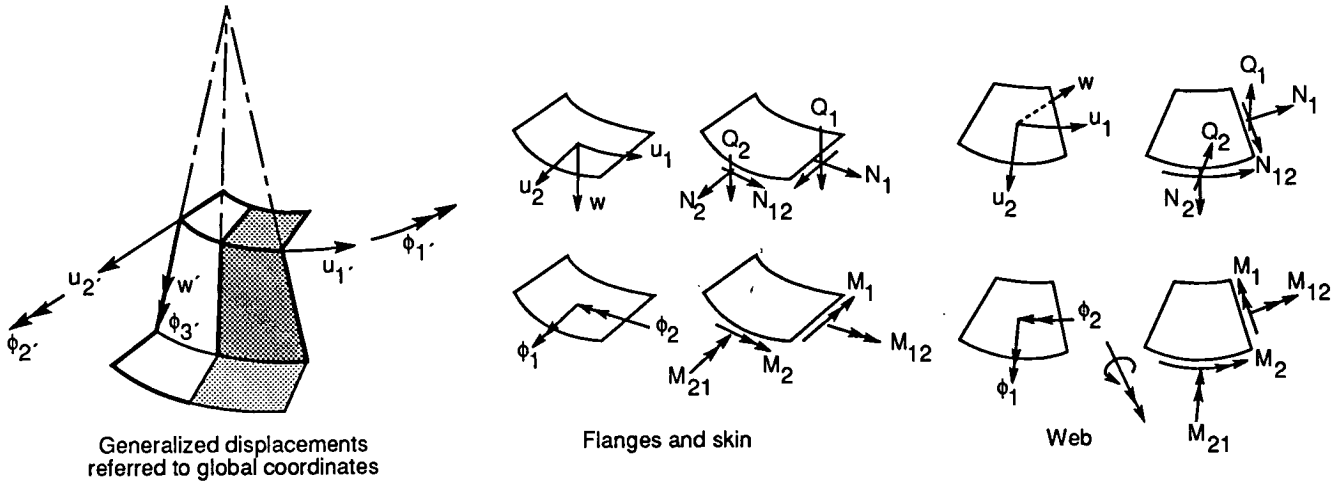

Figure 2. Sign convention for generalized displacements and stress resultants in two-dimensional model.

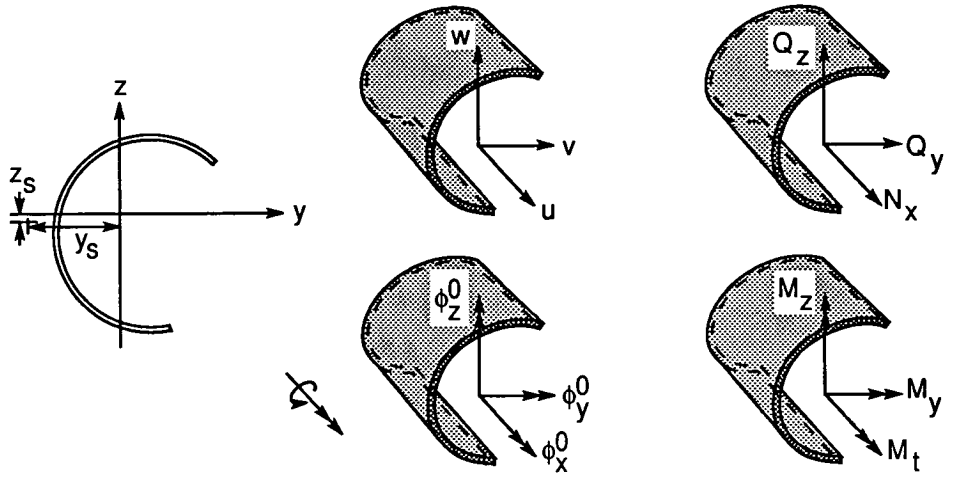

Figure 3. Sign convention for generalized displacements and stress resultants in one-dimensional model.

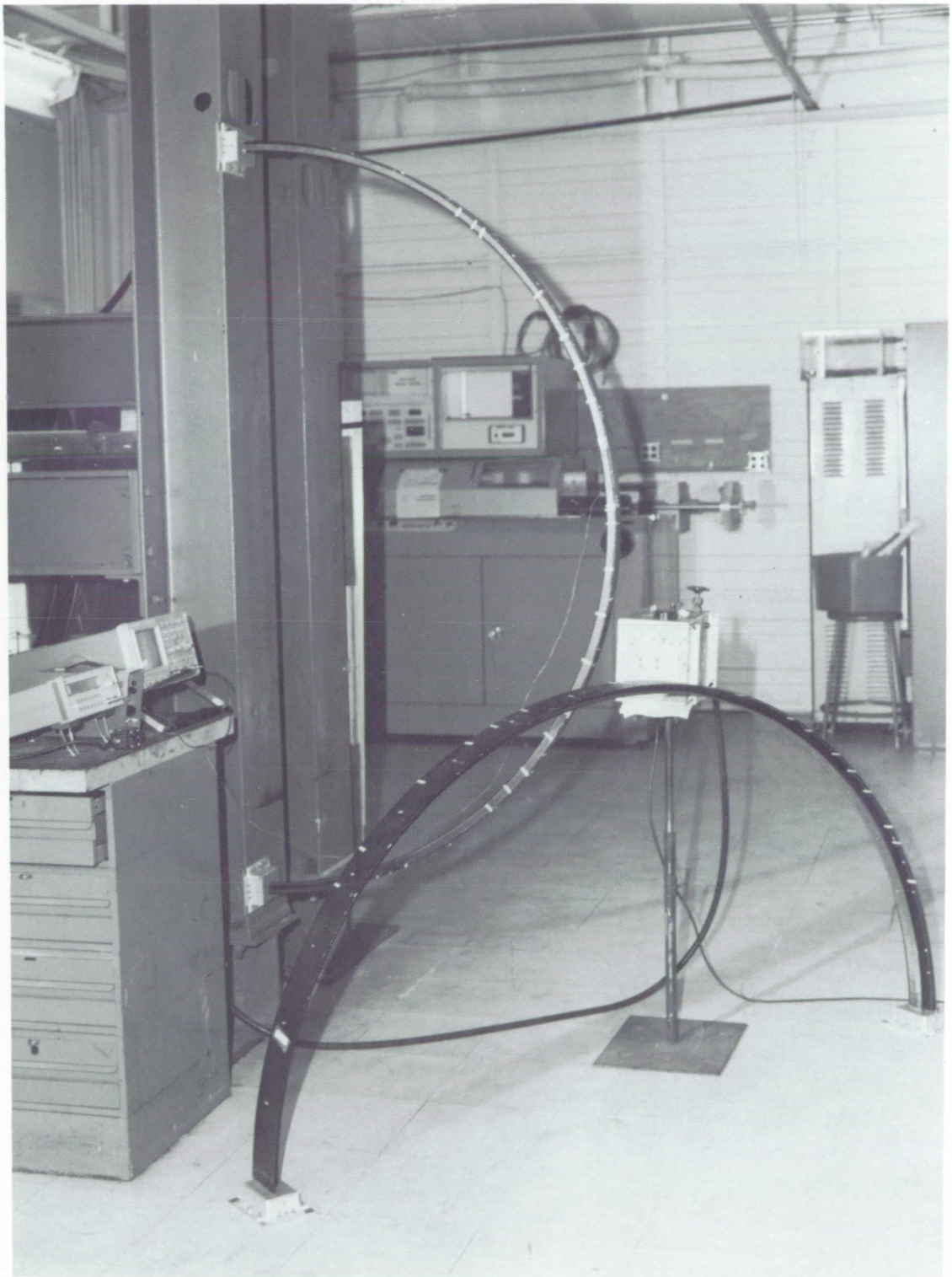

L-89-4693

Figure 4. Thin-walled semicircular graphite-epoxy specimens and equipment.

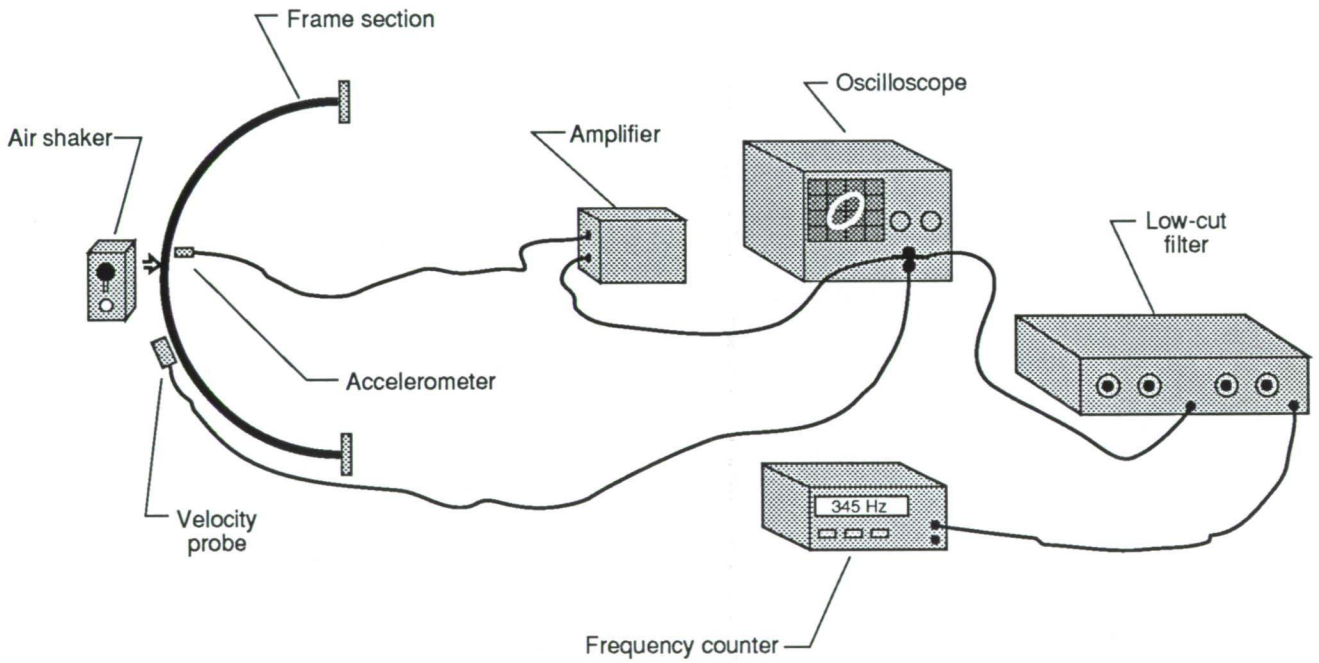

Figure 5. Schematic of test apparatus.

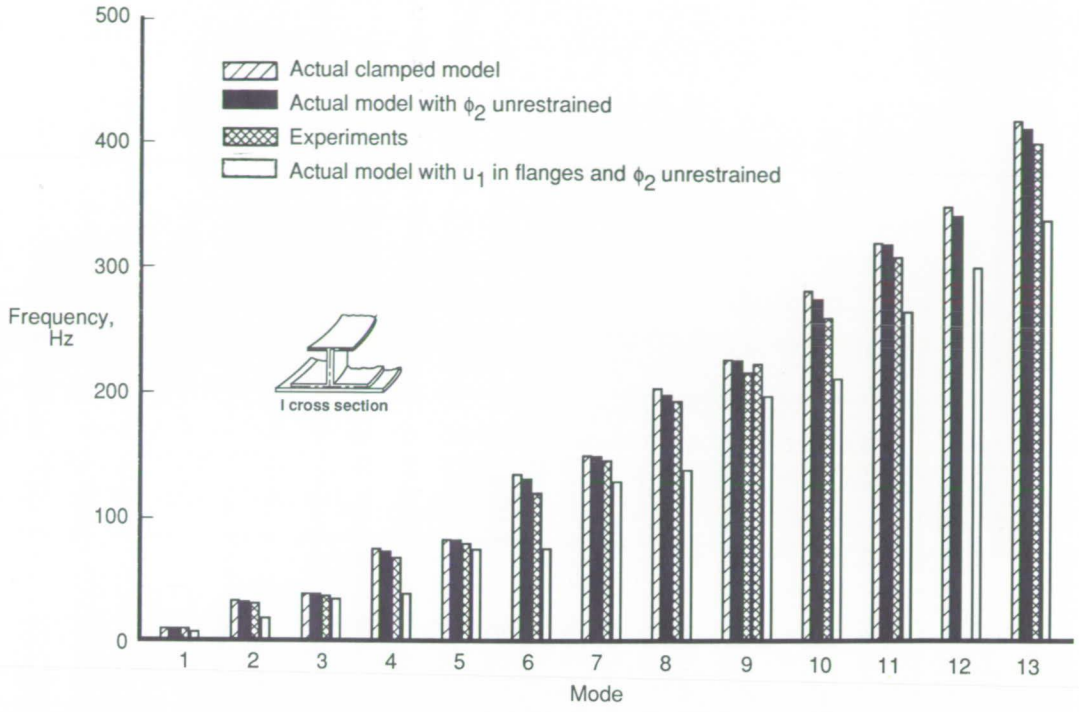

(a) Results for experimental and two-dimensional model.

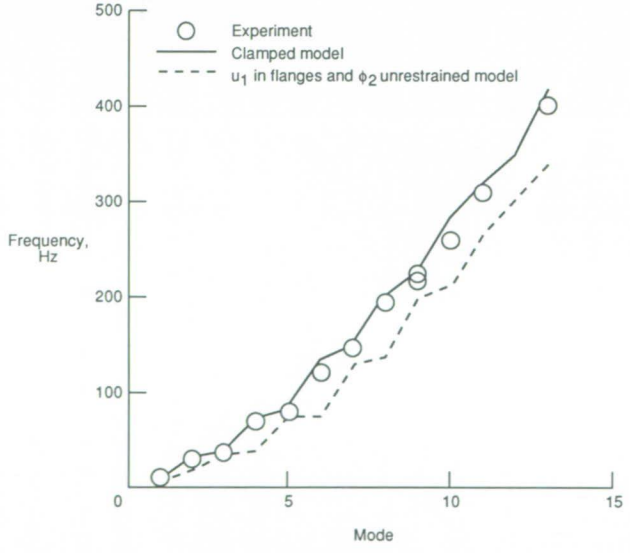

(b) Results for experimental and bounding two-dimensional model.

Figure 6. Comparison of finite-element and experimental frequencies for thin-walled composite frame with I cross section.

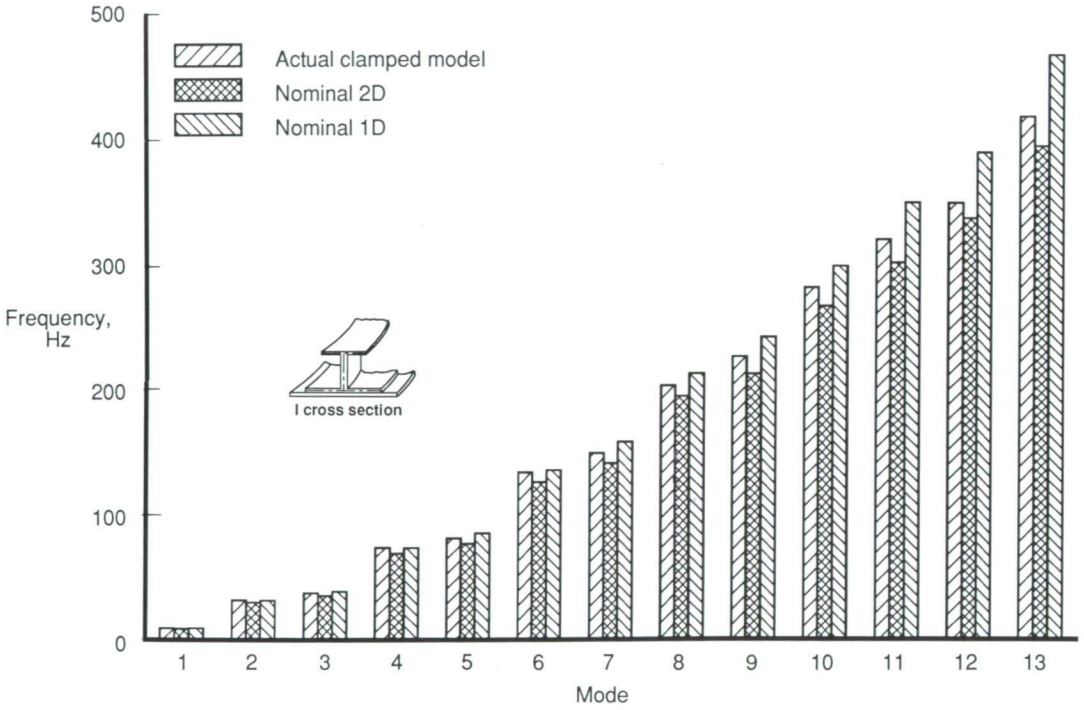

(c) Results for two-dimensional and one-dimensional-beam model.

Figure 6. Concluded.

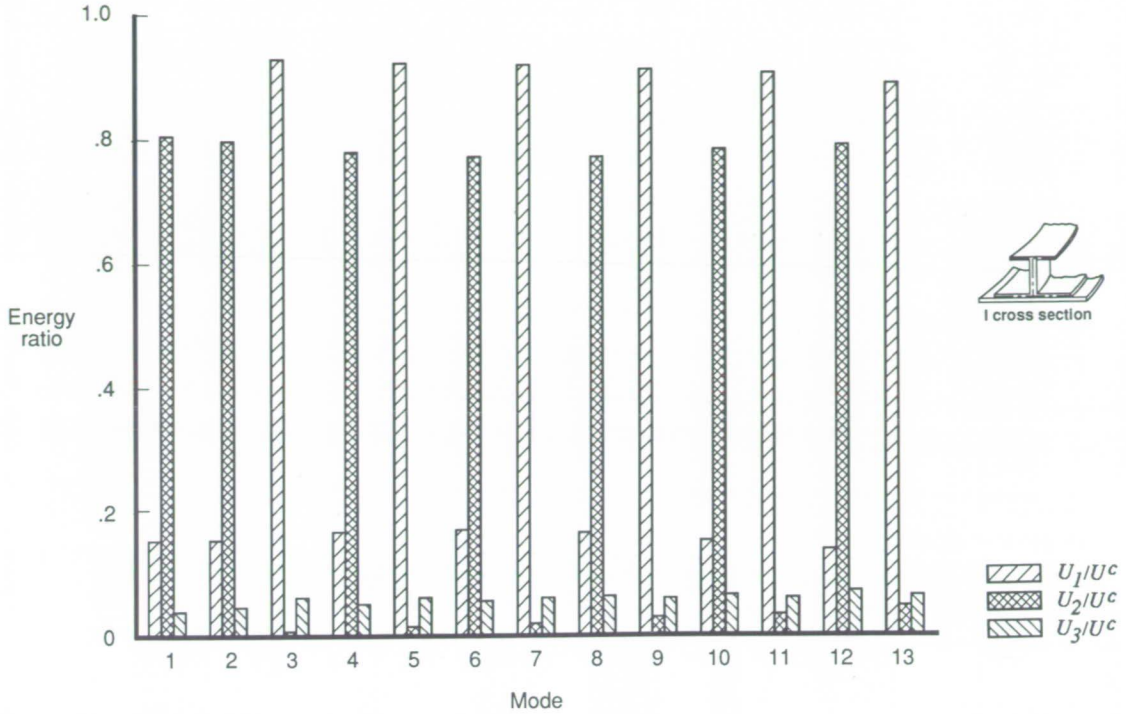

(a) U_1, U_2, and U_3.

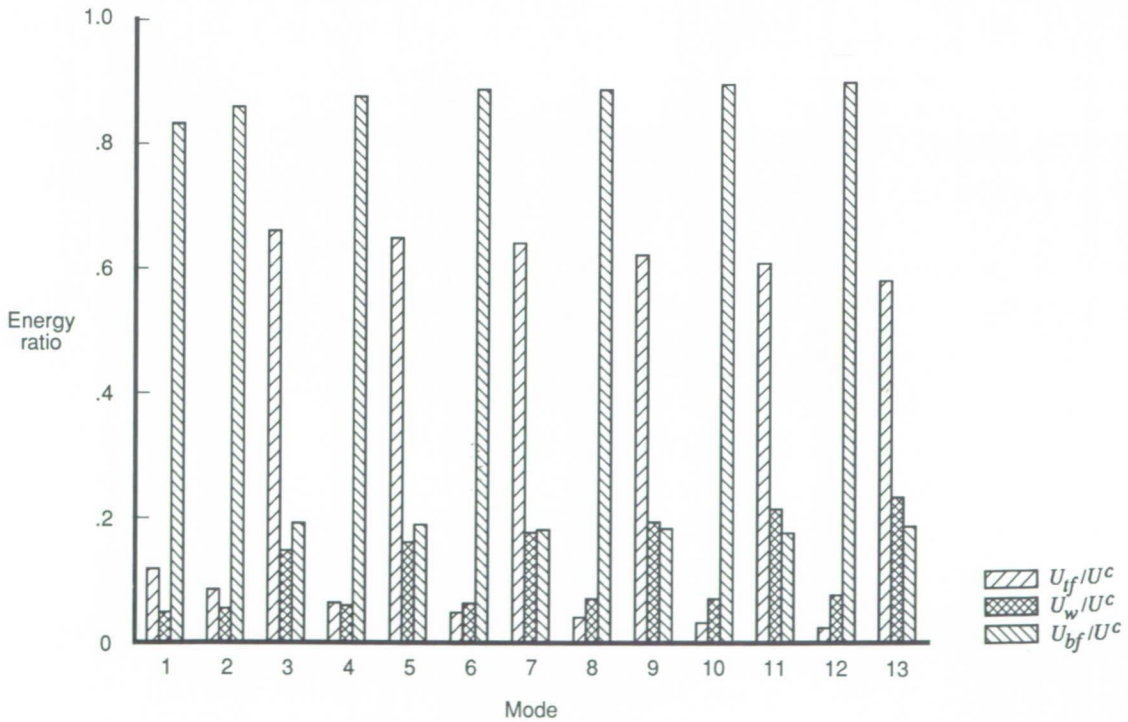

(b) U_{tf}, U_w, and U_{bf}.

Figure 7. Energy components in different vibration modes of thin-walled composite frame with I cross section.

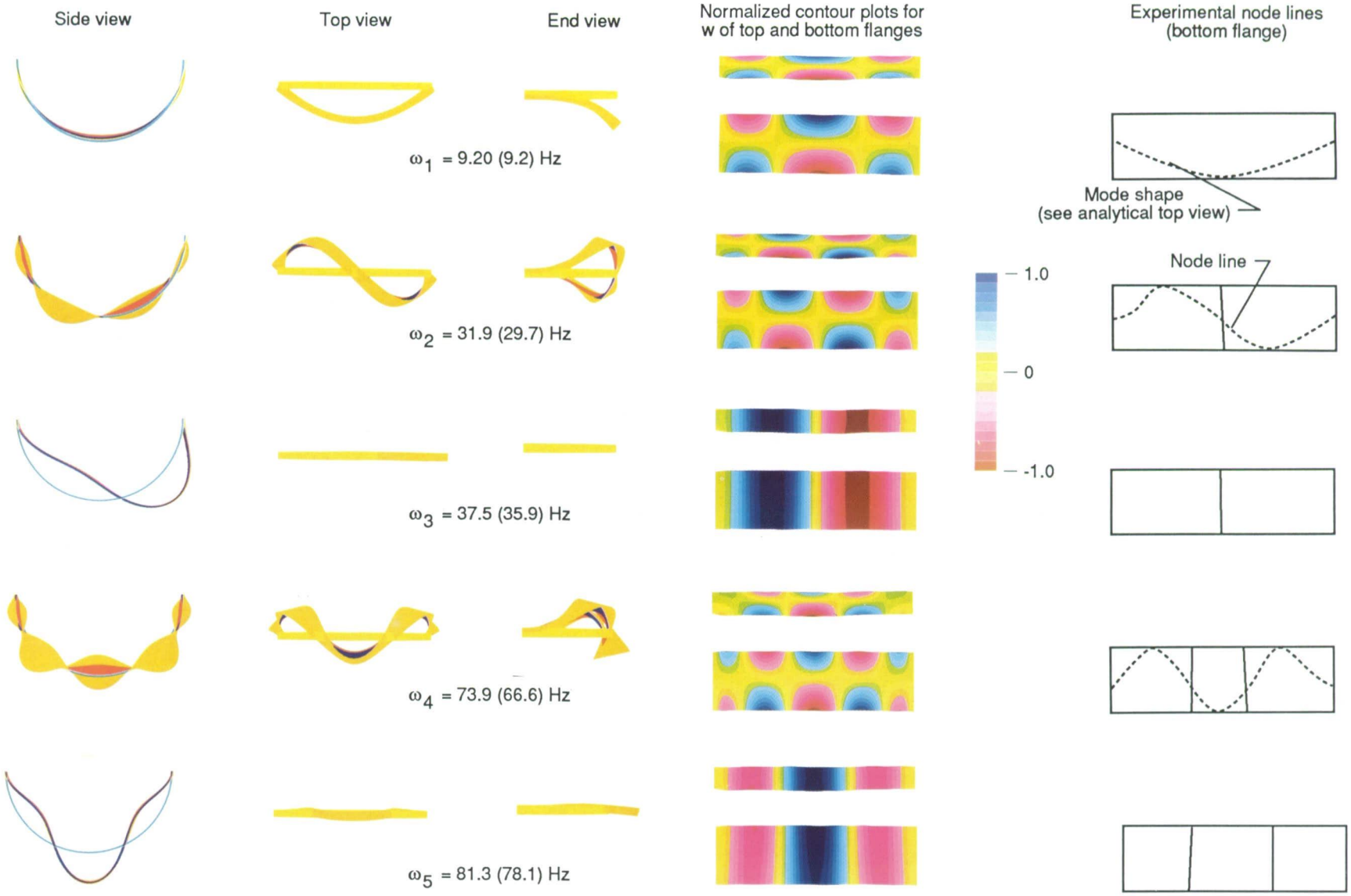

Figure 8. Mode shapes associated with lowest ten frequencies for thin-walled composite beam with I cross section. Numbers in parentheses are experimental frequencies. Other numbers are frequencies obtained by clamped finite-element model. The plots in the last two columns are not drawn to scale.

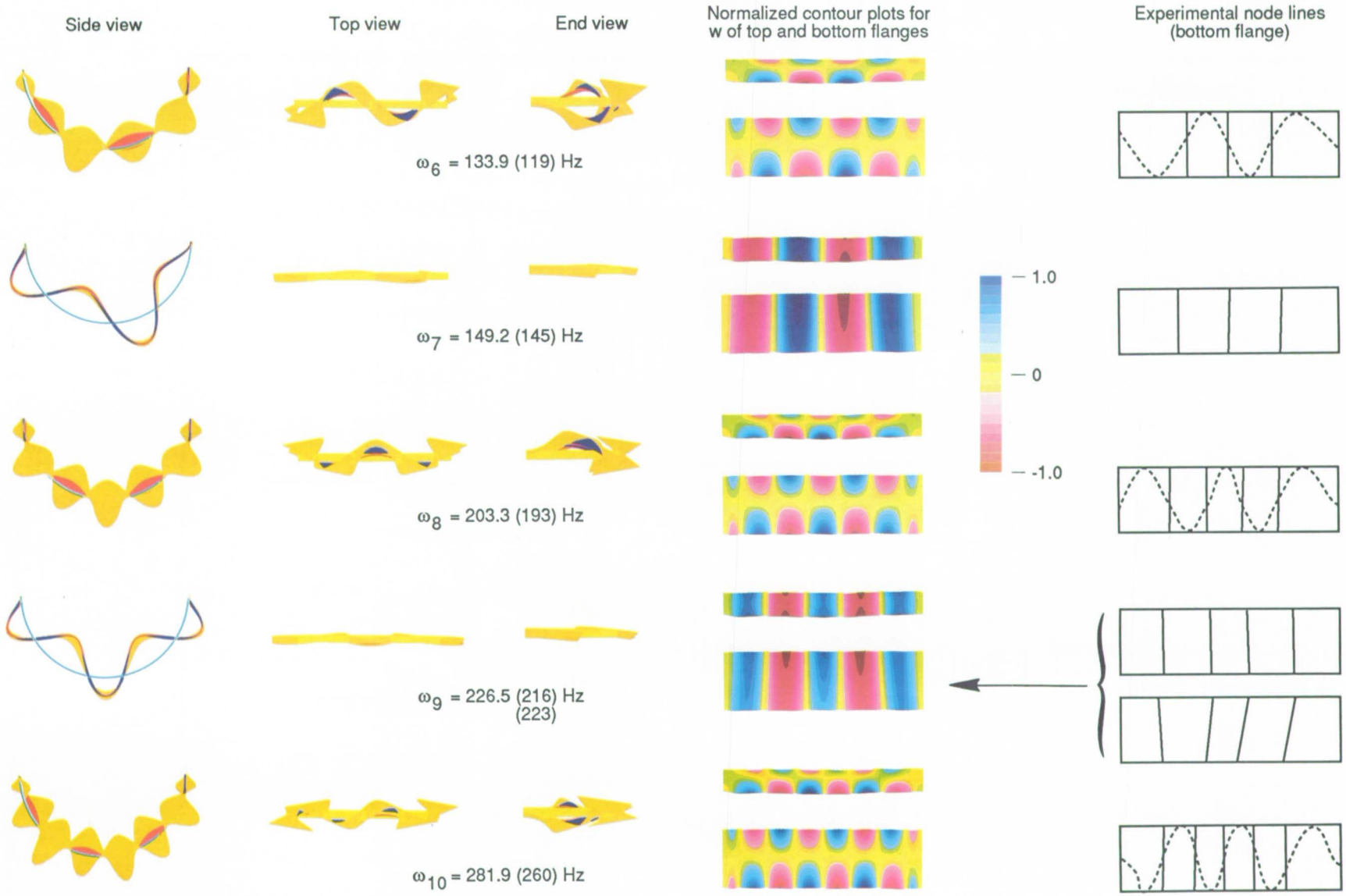

Figure 8. Concluded.

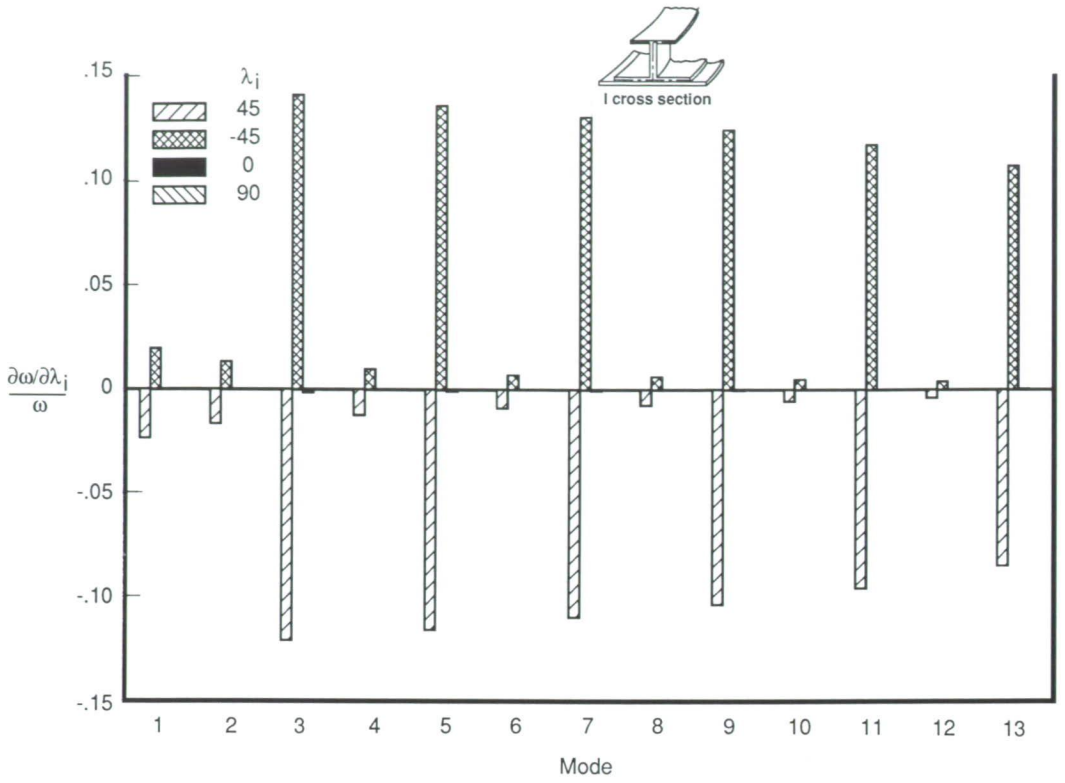

(a) Top flange.

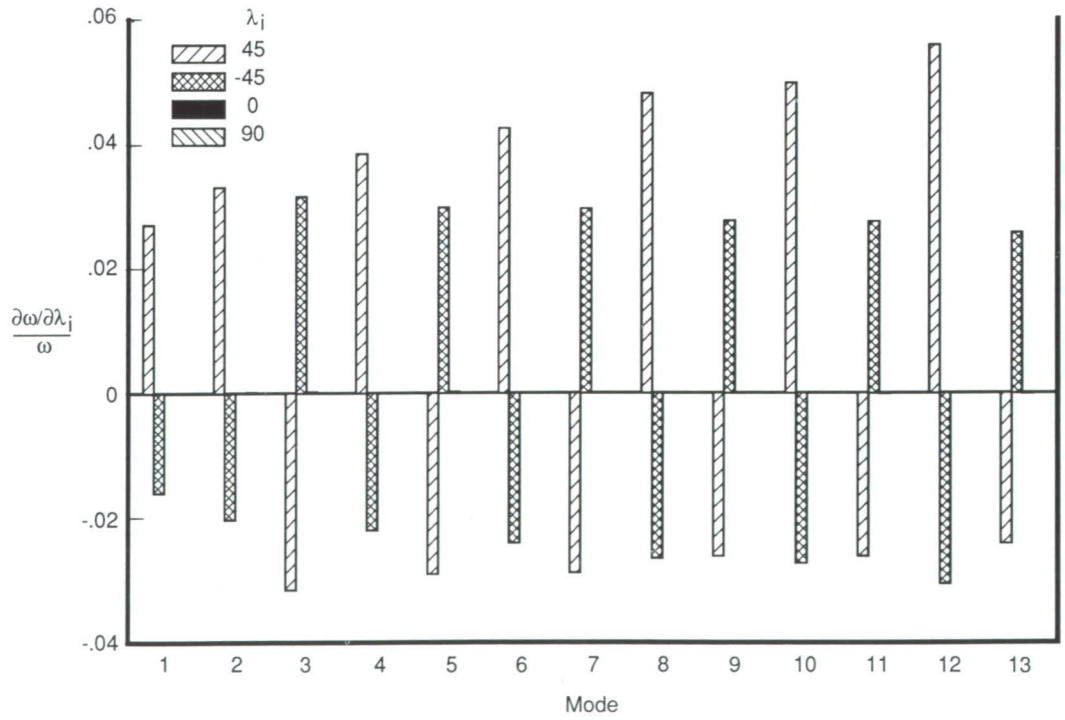

(b) Web.

Figure 9. Sensitivity of vibration frequencies to variations and fiber orientation of flanges and web for thin-walled composite frame with I cross section.

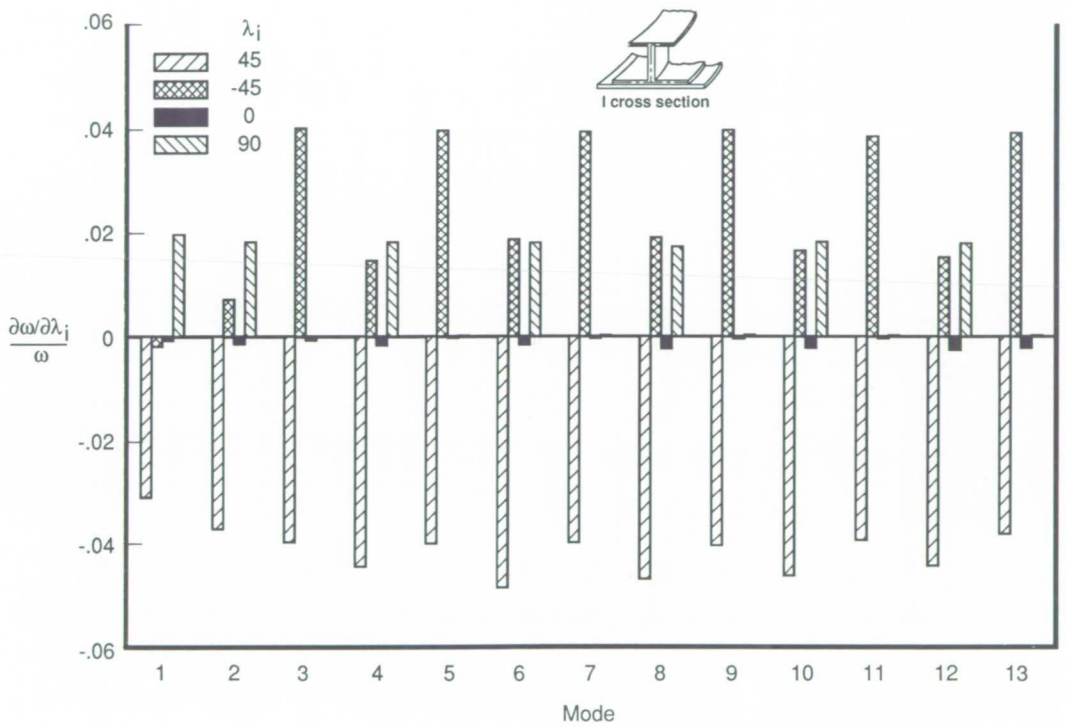

(c) Bottom flange and skin.

Figure 9. Concluded.

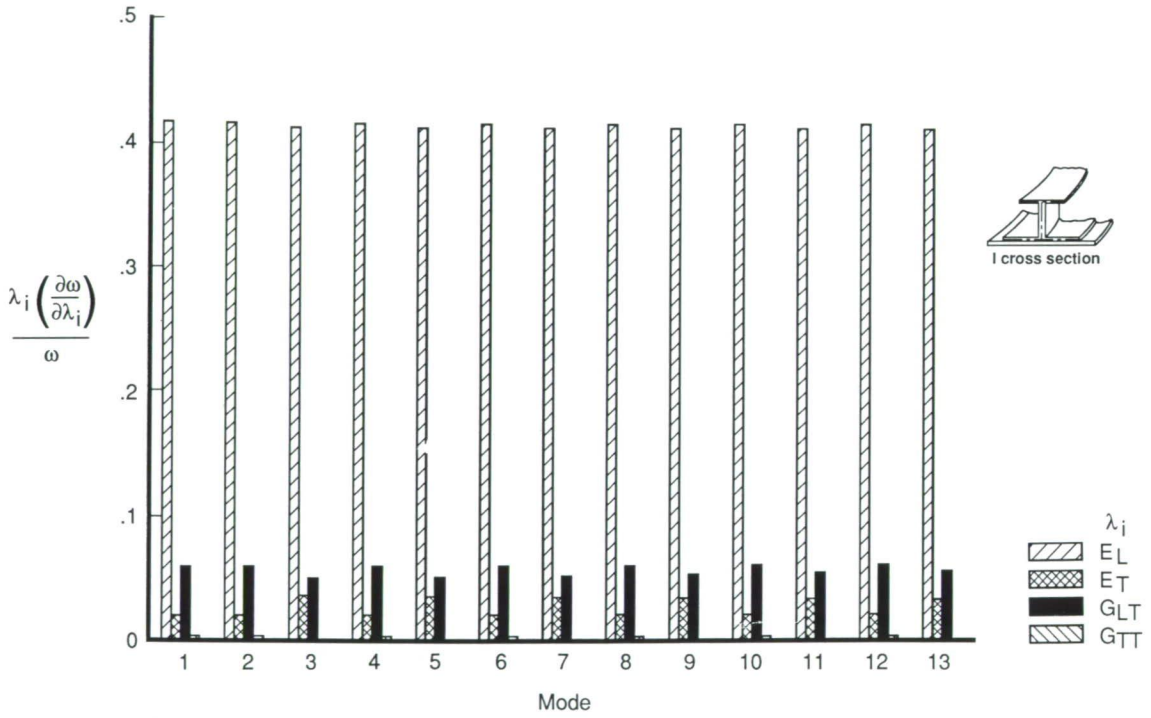

Figure 10. Sensitivity of vibration frequencies to variations in material characteristics of thin-walled composite frames with I cross section.

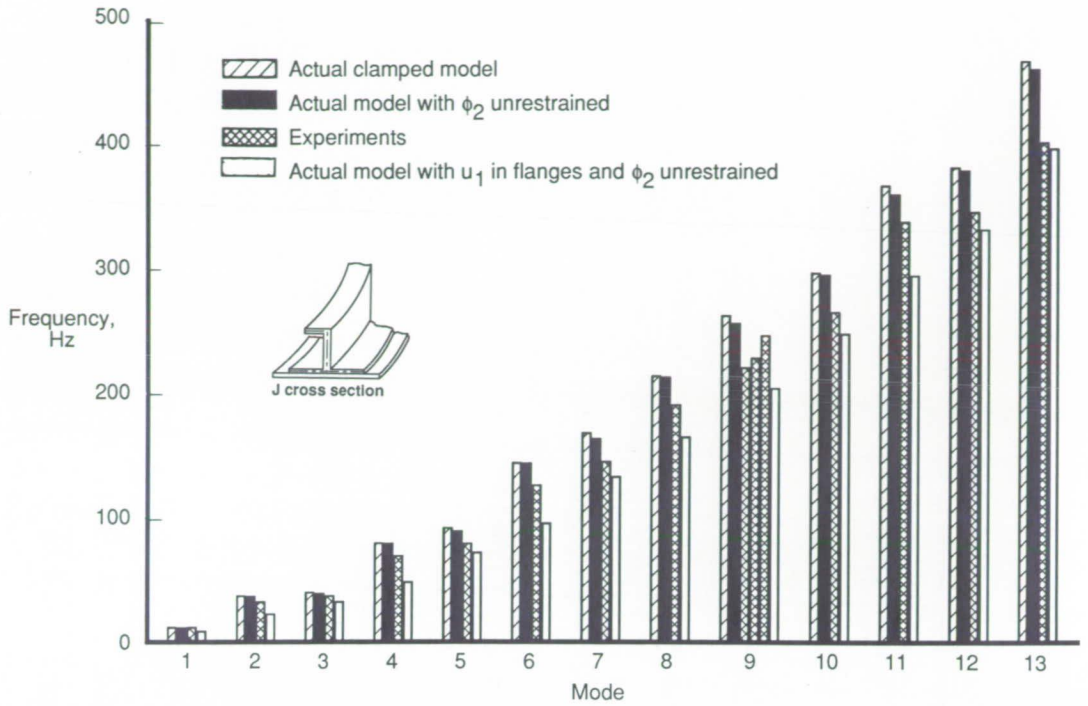

(a) Results for experimental and two-dimensional model.

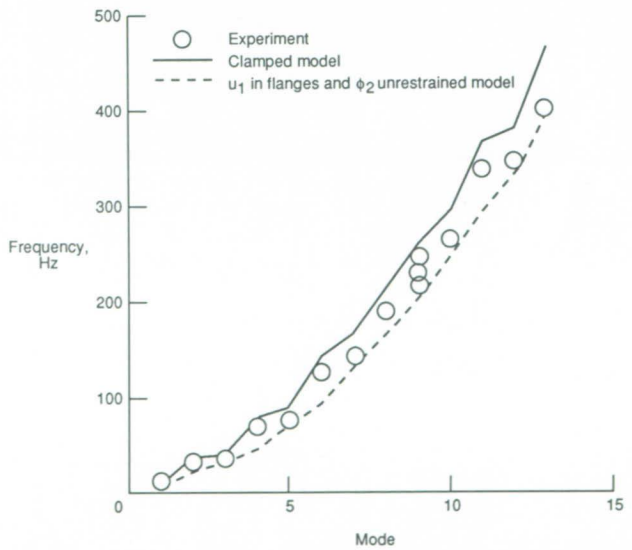

(b) Results for experimental and bounding two-dimensional model.

Figure 11. Comparison of finite-element and experimental frequencies for thin-walled composite frame with J cross section.

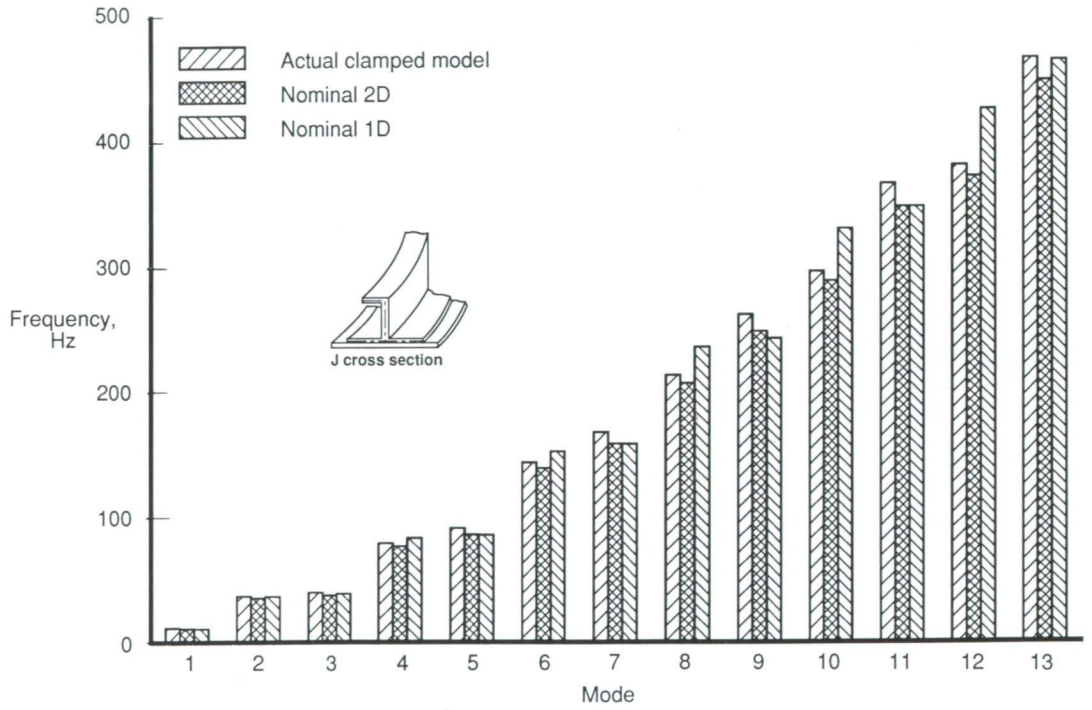

(c) Results for two-dimensional and one-dimensional-beam model.

Figure 11. Concluded.

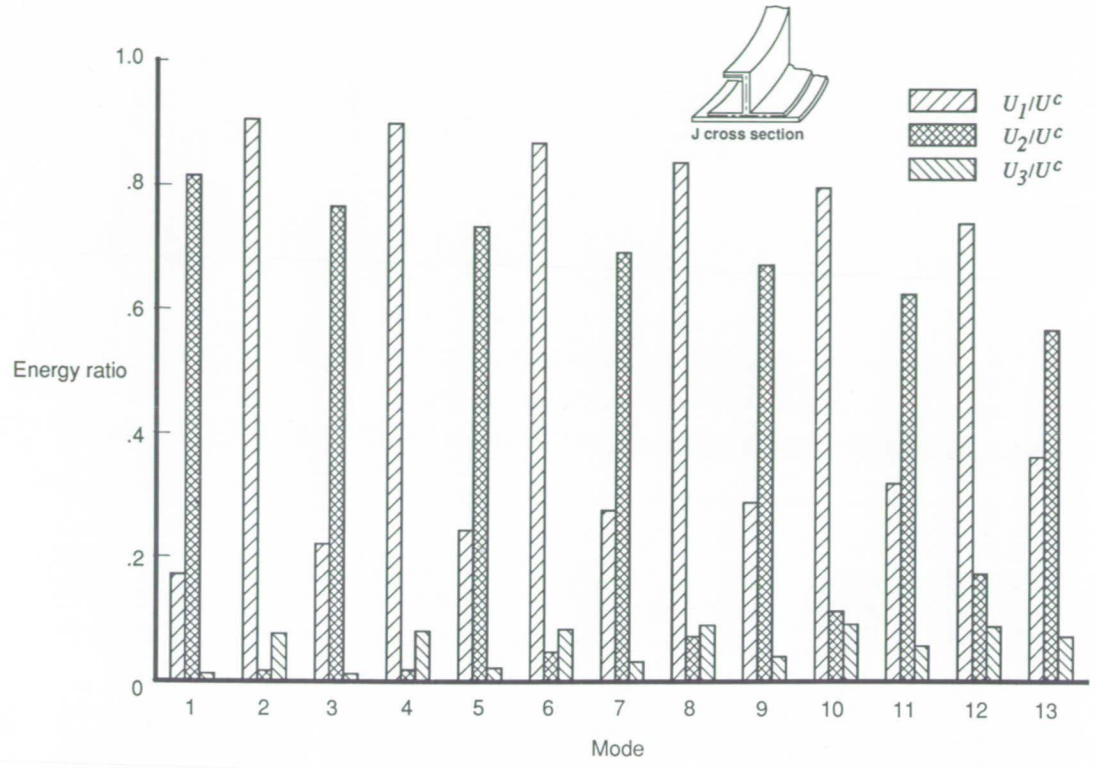

(a) U_1, U_2, and U_3.

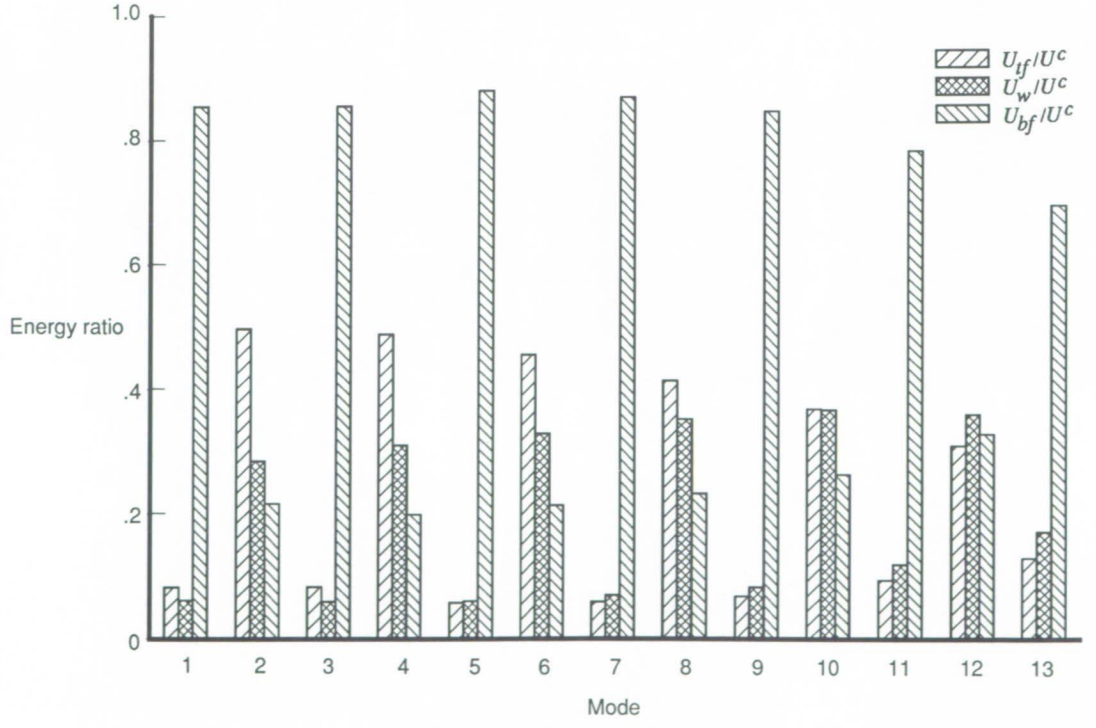

(b) U_{tf}, U_w, and U_{bf}.

Figure 12. Energy components in different vibration modes of thin-walled composite frame with J cross section.

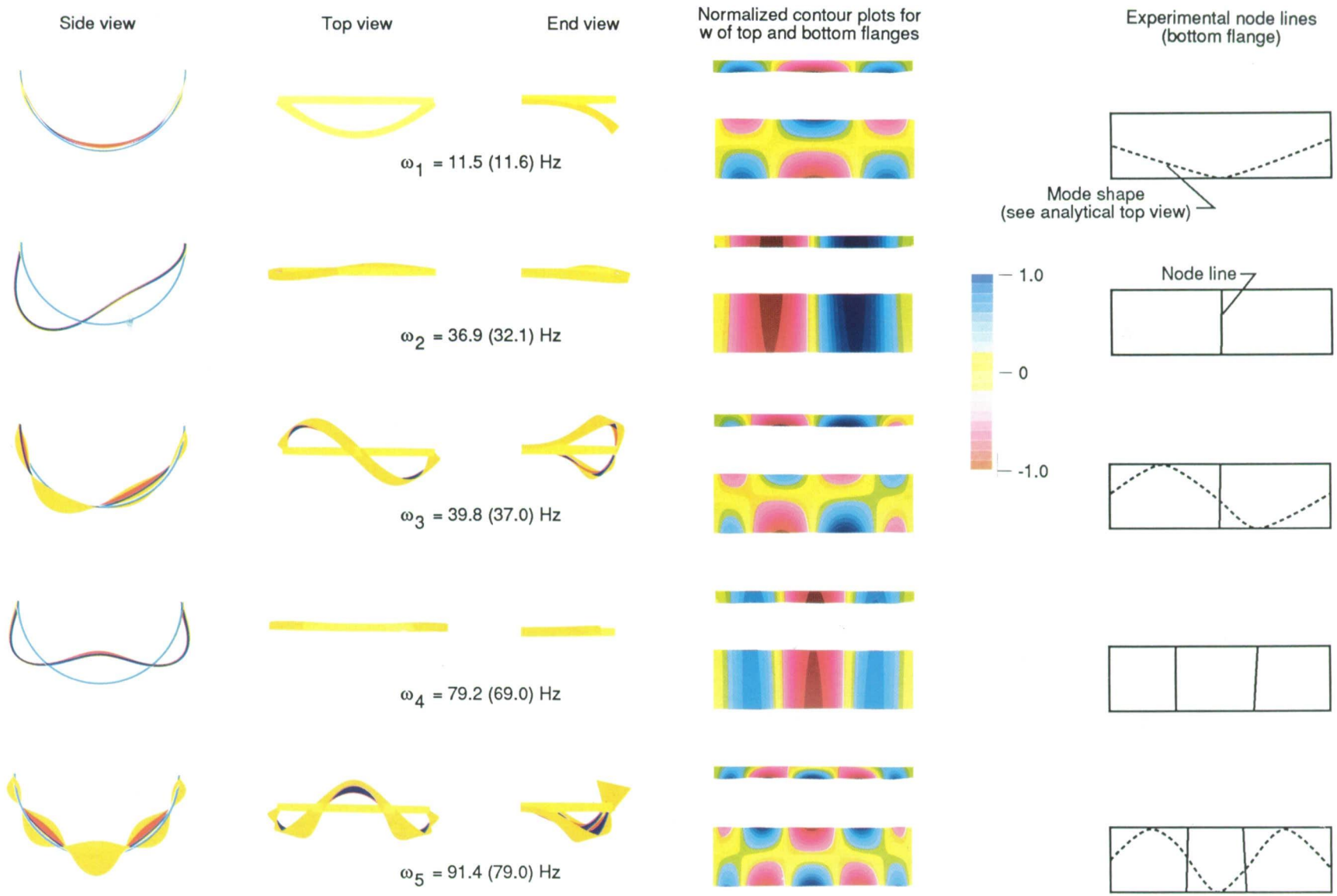

Figure 13. Mode shapes associated with lowest ten frequencies for thin-walled composite beam with J cross section. Numbers in parentheses are experimental frequencies. Other numbers are frequencies obtained by clamped finite-element model. The plots in the last two columns are not drawn to scale.

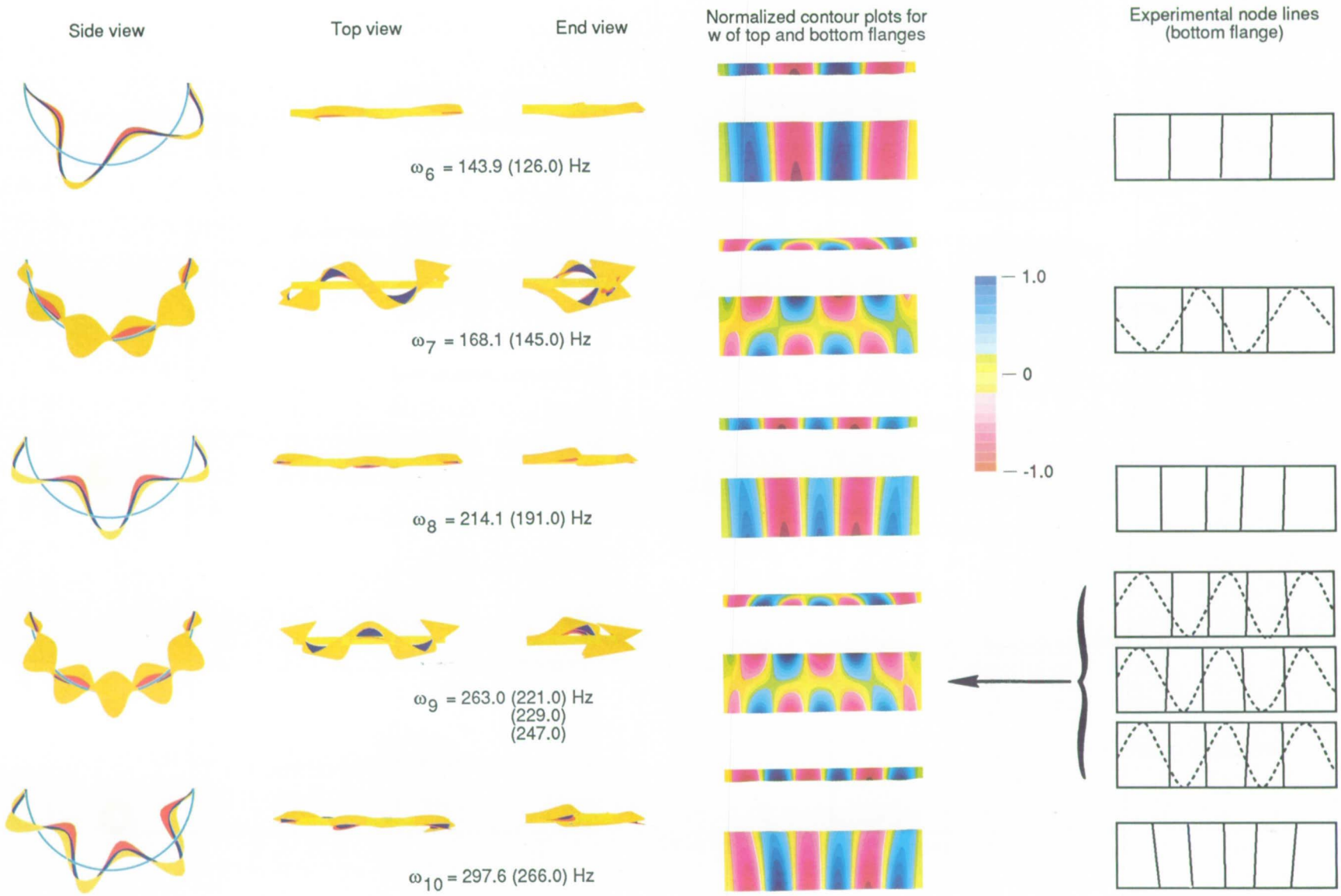

Figure 13. Concluded.

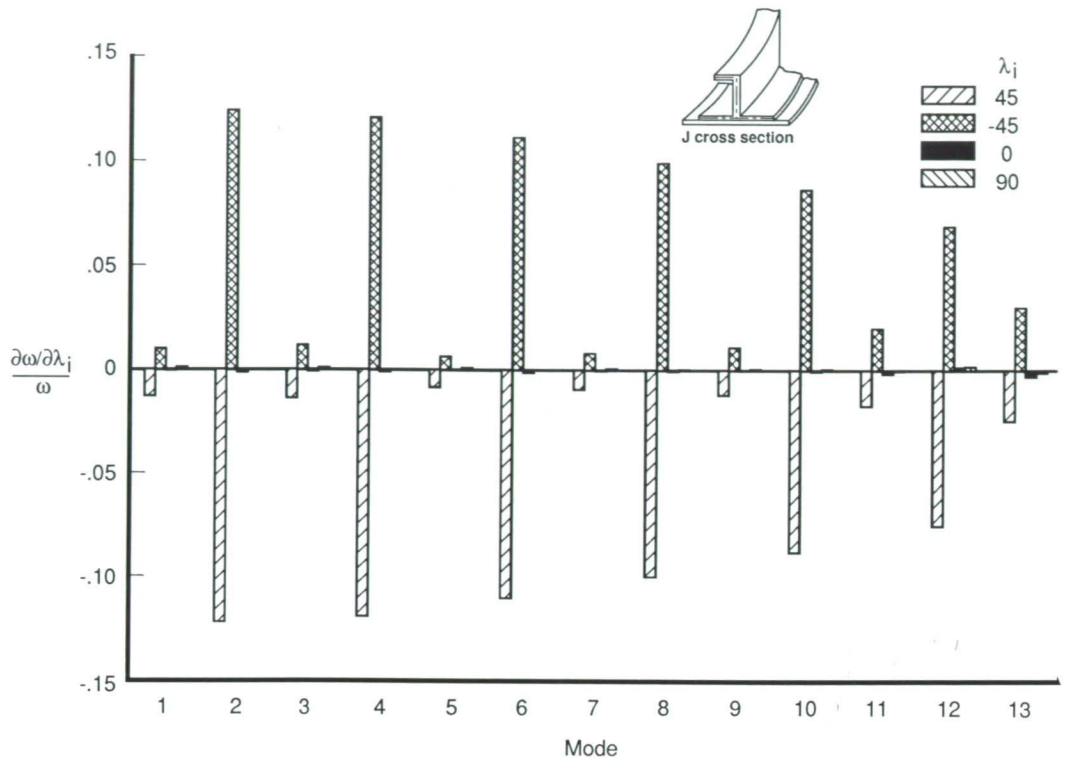

(a) Top flange.

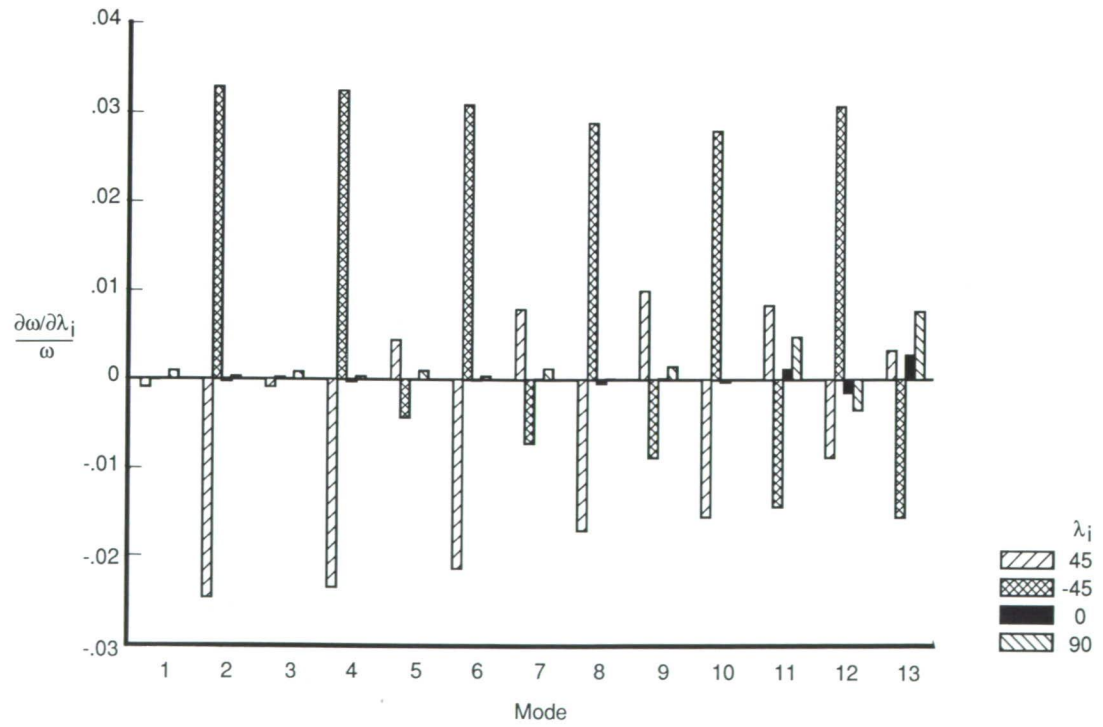

(b) Web.

Figure 14. Sensitivity of vibration frequencies to variations and fiber orientation of flanges and web for thin-walled composite frame with J cross section.

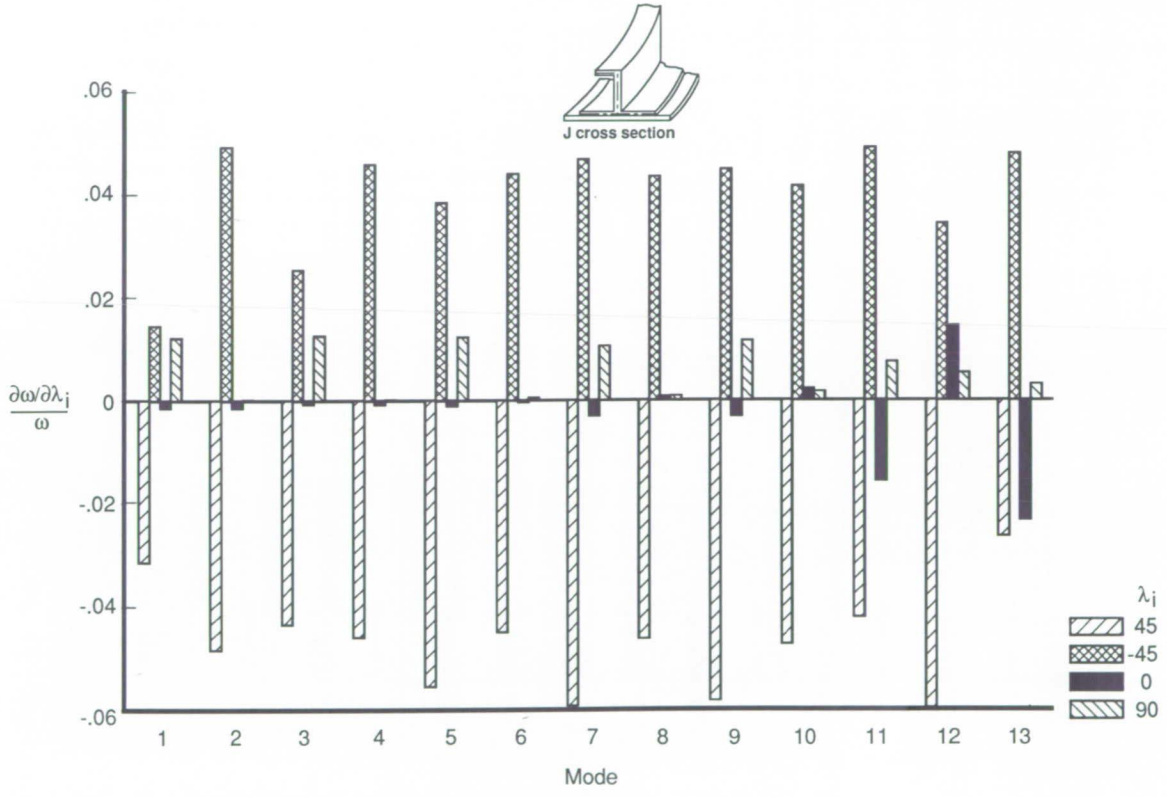

(c) Bottom flange and skin.

Figure 14. Concluded.

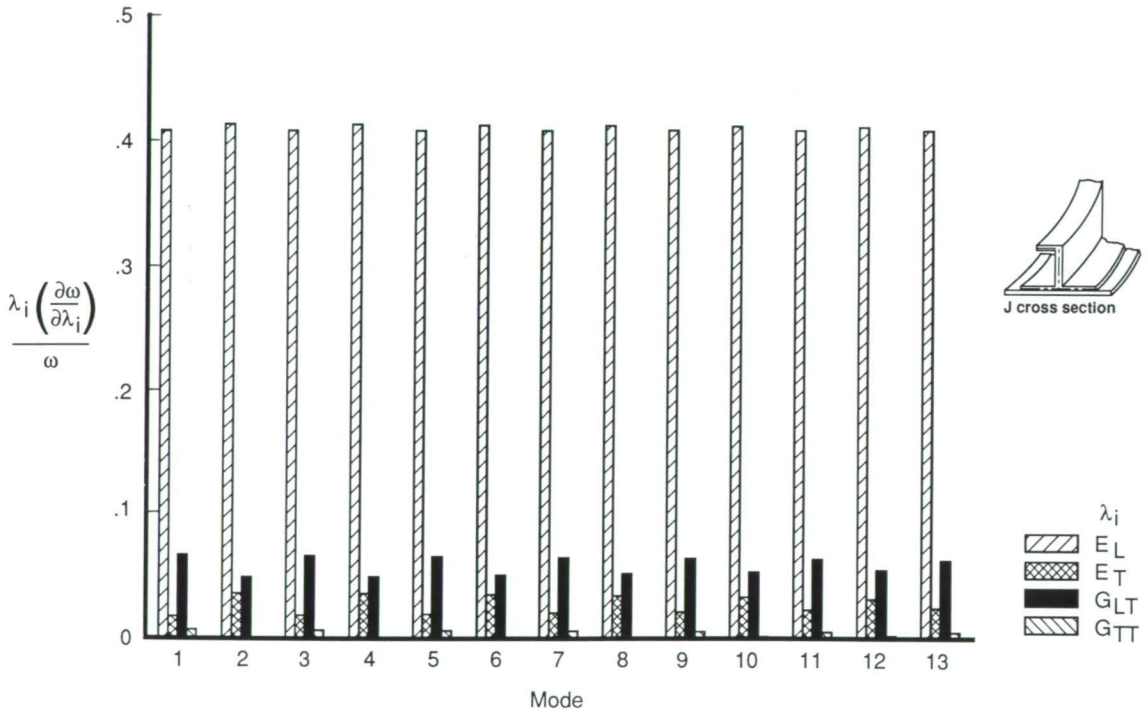

Figure 15. Sensitivity of vibration frequencies to variations in material characteristics of thin-walled composite frames with J cross section.

NASA
National Aeronautics and Space Administration

Report Documentation Page

1. Report No.	2. Government Accession No.	3. Recipient's Catalog No.
NASA TP-3010		

4. Title and Subtitle	5. Report Date
Free Vibrations of Thin-Walled Semicircular Graphite-Epoxy Composite Frames	November 1990
	6. Performing Organization Code
7. Author(s)	8. Performing Organization Report No.
Ahmed K. Noor, Huey D. Carden, and Jeanne M. Peters	L-16726
9. Performing Organization Name and Address	10. Work Unit No.
NASA Langley Research Center Hampton, VA 23665-5225	505-63-01-11
	11. Contract or Grant No.
12. Sponsoring Agency Name and Address	13. Type of Report and Period Covered
National Aeronautics and Space Administration Washington, DC 20546-0001	Technical Paper
	14. Sponsoring Agency Code

15. Supplementary Notes

Ahmed K. Noor and Jeanne M. Peters: The George Washington University, Joint Institute for Advancement of Flight Sciences, Langley Research Center, Hampton, Virginia.
Huey D. Carden: Langley Research Center, Hampton, Virginia.

16. Abstract

A detailed study is made of the effects of variations in lamination and material parameters of thin-walled composite frames on their vibrational characteristics. The structures considered are semicircular thin-walled frames with I and J sections. The flanges and webs of the frames are modeled by using two-dimensional shell and plate finite elements. A mixed formulation is used with the fundamental unknowns consisting of both the generalized displacements and stress resultants in the frame. The frequencies and modes predicted by the two-dimensional finite-element model are compared with those obtained from experiments, as well as with the predictions of a one-dimensional, thin-walled-beam, finite-element model. A detailed study is made of the sensitivity of the vibrational response to variations in the fiber orientation, material properties of the individual layers, and boundary conditions.

17. Key Words (Suggested by Authors(s))	18. Distribution Statement
Composite-frame vibrations Experimental and analytical vibrations Composite structures and vibrations Composite analysis	Unclassified—Unlimited Subject Category 39

19. Security Classif. (of this report)	20. Security Classif. (of this page)	21. No. of Pages	22. Price
Unclassified	Unclassified	41	A03

NASA FORM 1626 OCT 86 NASA-Langley, 1990
For sale by the National Technical Information Service, Springfield, Virginia 22161-2171

National Aeronautics and
Space Administration
Code NTT-4

Washington, D.C.
20546-0001